Parameterization of γ, $e^{\pm}$ and Neutrino Spectra Produced by $p-p$ Interaction in Astronomical Environment

Tuneyoshi Kamae[1], Niklas Karlsson[2], Tsunefumi Mizuno[3], Toshinori Abe[4], Tatsumi Koi

Stanford Linear Accelerator Center, Menlo Park, CA 94025

kamae@slac.stanford.edu

ABSTRACT

We present the yield and spectra of stable secondary particles (γ, $e^{\pm}$, ν_e, $\bar{\nu}_e$, ν_μ, and $\bar{\nu}_\mu$) of $p-p$ interaction in parameterized formulae to facilitate calculations involving them in astronomical environments. The formulae are derived from the up-to-date $p-p$ interaction model by Kamae et al. (2005), which incorporates the logarithmically rising inelastic cross section, the diffraction dissociation process, and the Feynman scaling violation. To improve fidelity to experimental data in lower energies, two baryon resonance contributions have been added: one representing $\Delta(1232)$ and the other representing multiple resonances around 1600 MeV/c^2. The parametrized formulae predict that all secondary particle spectra be harder by about 0.05 in power-law indices than that of the incident proton and their inclusive cross-sections be larger than those predicted by $p-p$ interaction models based on the Feynman scaling.

Subject headings: cosmic rays — galaxies: jets — gamma-rays: theory — ISM: general — neutrinos — supernovae: general

1. Introduction

Gamma-ray emission due to neutral pions produced by proton-proton interaction has long been predicted from the Galactic ridge, supernova remnants (SNRs), active galactic nucleus (AGN) jets, and other astronomical sites (Hayakawa 1969; Stecker 1971; Murthy & Wolfendale

---

[1] Also with Kavli Institute for Particle Astrophysics and Cosmology, Stanford University, Menlo Park, CA 94025

[2] Visiting scientist from Royal Institute of Technology, SE-10044 Stockholm, Sweden

[3] Present address: Department of Physics, Hiroshima University, Higashi-Hiroshima, Japan 739-8511

[4] Present address: Department of Physics, University of Tokyo, Tokyo, Japan 113-0033

1986; Schönfelder 2001; Schlickeiser 2002; Aharonian 2004; Aharonian et al. 2004). High energy neutrinos produced by $p-p$ interaction in AGN jets will soon be detected with large-scale neutrino detectors that are under construction (Halzen 2005). Spectra of these gamma-rays, neutrinos, and other secondaries depend heavily on the incident proton spectrum, which is unknown and needs to be derived, in almost all cases, from the observed spectra themselves. Such analyses often involve iterative calculations with many trial proton spectra. The parameterized model presented here is aimed to improve accuracy of such calculations.

Among the secondaries of $p - p$ interaction in astronomical environment, gamma-rays have been best studied. The p-p interaction is one of the two dominant gamma-ray emission mechanisms in the sub-GeV to multi-TeV range, the other being Compton up-scattering of low energy photons by high energy electrons. Gamma-rays in this energy range have been detected from pulsars, the Galactic Ridge, SNRs, blazars and other source categories (Stecker 1971; Murthy & Wolfendale 1986; Ong 1998; Schönfelder 2001; Weekes 2003; Aharonian 2004).

High energy gamma-rays from AGN jets are interpreted as mostly due to the inverse Compton up-scattering of low-energy photons by multi-TeV electrons. Observed radio and X-ray spectra match those of synchrotron radiation by these electrons. Synchronicity in variability between the observed X-ray and gamma-ray fluxes has given strong support for the inverse Compton up-scattering scenario (Ong 1998; Schönfelder 2001; Schlickeiser 2002; Aharonian 2004). For some AGN jets, the above scenario does not work well, and $p - p$ interaction has been proposed as an alternative mechanism (Mücke & Protheroe 2001; Mücke et al. 2003; Böttcher & Reimer 2004).

High energy gamma-rays detected by COS-B and EGRET from the Galactic Ridge, on the other hand, are interpreted as predominantly due to neutral pions produced by interaction of protons and nuclei with the interstellar matter (ISM; Stecker 1973; Strong et al. 1978, 1982, 2000; Stephens & Badhwar 1981; Mayer-Hasselwander et al. 1982; Bloemen et al. 1984; Bloemen 1985; Dermer 1986a; Stecker 1990; Hunter et al. 1997; Mori 1997; Stanev 2004). The measured gamma-ray flux and spectral shape (Hunter et al. 1997) have been viewed as the key attestation to this interpretation. It is also known that inverse Compton scattering contributes significantly to the Galactic Ridge gamma-ray emission (Murthy & Wolfendale 1986; Strong et al. 2000; Schönfelder 2001).

In the past two years, several SNRs, including RX J1713-3946 and RX J0852-4622, have been imaged in the TeV band with an angular resolution around 0.1° by H.E.S.S. (Aharonian et al. 2004b,c; Aharonian 2005). A smooth featureless spectrum, suggestive of synchrotron radiation by multi-TeV electrons, has been detected in the X-ray band from RX J1713-3946 (Koyama et al. 1997; Slane et al. 1999; Uchiyama et al. 2003) and RX J0852-

4622 (Tsunemi et al. 2000; Iyudin et al. 2005). The measured TeV gamma-ray fluxes and spectra, however, do not agree well with those predicted by the inverse Compton scenario (see, e.g., the analysis in Uchiyama et al. (2003)). Several authors have proposed that the TeV gamma-rays are possibly due to interaction of accelerated protons with the ISM (Berezhko & Volk 2000; Enomoto et al. 2002; Aharonian 2004; Katagiri et al. 2005).

Higher precision data are expected, in the GeV range, from GLAST Large Area Telescope (GLAST-LAT 2005)[1] and, in the TeV range, from the upgraded Air Cherenkov Telescopes (Aharonian et al. 2004): they will soon test applicability of the inverse Compton upscattering and the proton interaction with ISM for various astronomical gamma-ray sources. In many objects, secondary electrons and positrons may produce fluxes of hard X-rays and low-energy gamma-rays detectable with high-sensitivity instruments aboard *Integral*, *Swift*, *Suzaku*, and *NuSTAR*.[2] The formulae given here will give fluxes and spectra of these secondary particles for arbitrary incident proton spectrum.

This work is an extension of that by Kamae et al. (2005), where up-to-date knowledge of the π^0 yield in the $p - p$ inelastic interaction has been used to predict the Galactic diffuse gamma-ray emission. The authors have found that past calculations (Stecker 1970, 1973, 1990; Strong et al. 1978; Stephens & Badhwar 1981; Dermer 1986a,b; Mori 1997; Strong et al. 2000) had left out the diffractive interaction and the Feynman scaling violation in the non-diffractive inelastic interaction. Another important finding by them is that most previous calculations have assumed an energy-independent $p - p$ inelastic cross-section of about 24 mb for $T_p \gg 10$ GeV, whereas recent experimental data have established a logarithmic increase with the incident proton energy. Updating these shortfalls has changed the prediction on the gamma-ray spectrum in the GeV band significantly: the gamma-ray power-law index is harder than that of the incident proton; and the GeV−TeV gamma-ray flux is significantly larger than that predicted on the constant cross-section and Feynman scaling (Kamae et al. 2005). The model by Kamae et al. (2005) will hereafter be referred to as model A.

Model A does not model $p - p$ interaction accurately near the pion production threshold. To improve prediction of gamma-rays, electrons, and positrons produced near the pion production threshold, two baryon resonance excitation components have bee added to model A: $\Delta(1232)$, representing the Δ resonance, and res(1600), representing resonances around

---

[1]GLAST Large Area Telescope, http://www-glast.stanford.edu.

[2]See *INTEGRAL* Web site, http://sci.esa.int/esaMI/Integral, the *NuSTAR* Web site, http://www.nustar.caltech.edu, the *Suzaku* Web site http://www.isas.jaxa.jp/e/enterp/missions/astro-e2, and the *Swift* Web site, http://swift.gsfc.nasa.gov/docs/swift.

1600 MeV/c^2. We note here that $\Delta(1232)$ is the most prominent and lightest Baryon resonance excited in $p - p$ interaction. It has a mass of 1.232 GeV/c^2 and a width of about 0.12 GeV/c^2, and decays to a nucleon (proton or neutron) and a pion ($\pi^{+,0,-}$). The other resonance, res(1600), is assumed to decay to a nucleon and two pions. Introduction of these contributions have necessitated adjustment of the model A at lower energies as described below. The readjusted model will be referred to as the "readjusted model A".

The parameterized model presented here exhibits all features of model A at higher energies (proton kinetic energy, $T_p > 3$ GeV) and reproduces experimental data down to the pion production threshold. The inclusive gamma-ray and neutrino cross-section formulae can be used to predict their yields and spectra for a wide range of incident proton spectrum. Formulae for electrons and positrons predict sub-TeV to multi-TeV secondary electrons and positrons supplied by $p - p$ interaction. We note that space-borne experiments such as PAMELA[3] will soon measure the electron and positron spectra in the sub-TeV energy range, where the secondaries of $p-p$ interaction may become comparable to the primary components (Müller 2001; Stephens 2001; DuVernois et al. 2001).

Due to paucity of experimental data and widely accepted modeling, we have not parameterized inclusive secondary cross-sections for $\alpha - p$ nor $p-$He nor $\alpha-$He interactions. We note that α-particles are known to make up about 7% by number of cosmic-rays observed near the Earth (Schlickeiser 2002) and that He to make up $\sim 10\%$ by number of interstellar gas. The total non $p - p$ contribution is comparable to that of $p - p$ contribution. The α-particle and He nucleus can be regarded, to a good approximation, as four independent protons beyond the resonance region ($T_p > 3$ GeV): the error introduced is expected to be less than 10% for high energy light secondary particles (Kamae et al. 2005).

Inclusion of α-particle as projectile and He nuclei as targets will change the positron-electron ratio significantly (about $10 - 15\%$) as discussed below. Fermi motion of nucleons and multiple nucleonic interactions in the nucleus are known to significantly affect pion production near the threshold and in the resonance region ($T_p < 3$ GeV; Crawford et al. 1980; Mårtensson et al. 2000); we acknowledge need for separate treatment of $p-$He, $\alpha - p$, and $\alpha-$He interactions in the future.

---

[3]See http://wizard.roma2.infn.it/pamela.

2. Monte Carlo Event Generation

The parameterization of the inclusive cross sections for γ, $e^{\pm}$, ν, and $\bar{\nu}$ has been carried out, separately, for non-diffractive, diffractive, and resonance-excitation processes, in three steps: First, the secondary particle spectra have been extracted out of events generated for mono-energetic protons (0.488 GeV $< T_p < 512$ TeV) based on the readjusted model A. We then fit these spectra with a common parameterized function, separately for non-diffractive, diffractive and resonance-excitation processes. In the third step, the parameters determined for mono-energetic protons are fitted as functions of proton energy, again separately for the three processes. The above procedure has been repeated for all secondary particle types.

The functional formulae often introduce tails extending beyond the energy-momentum conservation limits, which may produce artifacts when wide range spectral energy density ($E^2 d$flux$(\gamma)/dE$) is plotted. To eliminate such artifacts, we introduce another set of functions to impose the kinematic limits.

Several simulation programs have been used in model A (Kamae et al. 2005): for the high energy non-diffractive process ($T_p > 52.6$ GeV), Pythia 6.2 (Sjöstrand et al. 2001) with the multi-parton-level scaling violation option (Sjöstrand & Skands 2004);[4] for the lower energy non-diffractive process, the parameterized model by (Blattnig et al. 2000); for the diffractive part, the program by T. Kamae (2004, personal communication)[5]. In the readjusted model A, two programs to simulate two resonance-excitation components have also been added. Modeling of the two resonance components will be explained below.

3. Non-Diffractive, Diffractive, and Resonance-Excitation Cross-Sections

Experimental data on $p - p$ cross-sections are archived for a broad range of the incident proton energy and various final states. The total and elastic cross-sections have been compiled from those by Hagiwara et al. (2002), as shown in Figure 1. The two thin curves running through experimental data points in the figure are our eye-ball fits to the total and elastic cross sections. We then define the "empirical" inelastic cross section as the difference of the two curves to which the sum of non-diffractive, diffractive, $\Delta(1232)$-excitation, and res(1600)-excitation components are constrained. Typical errors in the empirical inelastic cross-section are 20% for $T_p < 3$ GeV and 10% for $T_p > 3$ GeV.

---

[4]See http://cepa.fnal.gov/CPD/MCTuning1 and http://www.phys.ufl.edu/~rfield/cdf.

[5]Diffractive process has been included in Pythia after the work began.

The four component cross sections of the readjusted model A and their sum are shown in Figures 1 and 2. The empirical inelastic cross section is shown by a series of small circles in Figure 2. The component cross sections take formulae given in equations (1) (non-diffractive), (2) (diffractive), (3) [$\Delta(1232)$] and (4) [res(1600)]. These are also shown in Figures 1 and 2.

We note that there is no clear experimental method separating the four components, especially at lower energies ($T_p < 20$ GeV). This ambiguity does not significantly affect the secondary particle fluxes, as long as the sum agrees with the total inelastic cross section and the total secondary inclusive cross sections agree with the corresponding experimental data.

The secondary particle spectra for a mono-energetic proton are normalized to the component cross sections given in equations (1), (2), (3) and (4) at the corresponding proton energy. We note that the non-diffractive component for $T_p < 52.6$ GeV is based on the formula by Blattnig et al. (2000), which is normalized to their π^0 inclusive cross section formula not to the total inelastic cross section. In the readjusted model A, this component cross section is defined by equation (1) and the π^0 inclusive cross section formula of Blattnig et al. (2000) has been redefined so that the sum of the four components reproduce the experimental π^0 inclusive cross section. The positive and negative pion inclusive cross sections are also redefined as products of our π^0 inclusive cross section and the ratio of the $\pi^{+,-}$ and π^0 inclusive cross sections given in Blattnig et al. (2000).
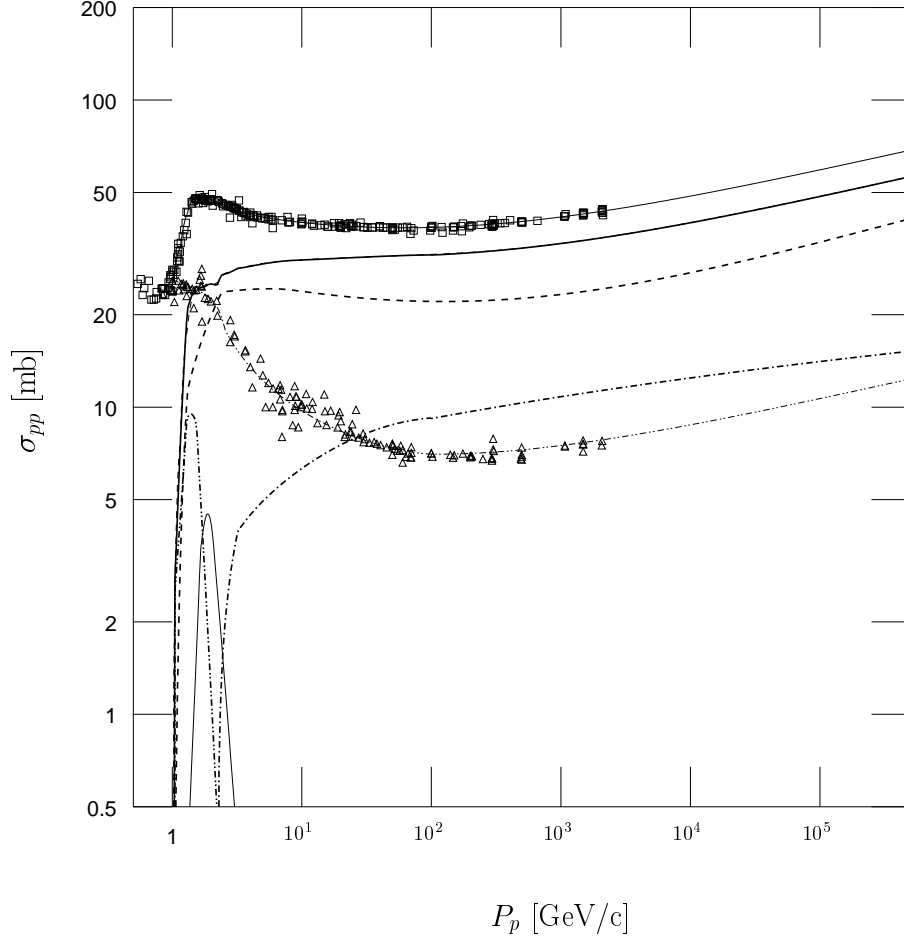
Fig. 1.— Experimental $p - p$ cross sections, as a function of proton momentum, and that of readjusted model A: experimental total (squares), experimental elastic (triangles), total inelastic (thick solid line), non-diffractive (dashed line), diffractive process (dot-dashed line), $\Delta(1232)$ (dotted line), and res(1600) (thin solid line). The total inelastic is the sum of the four components. The thin solid and dot-dot-dashed lines running through the two experimental data sets are eye-ball fits to the total and elastic cross sections, respectively.
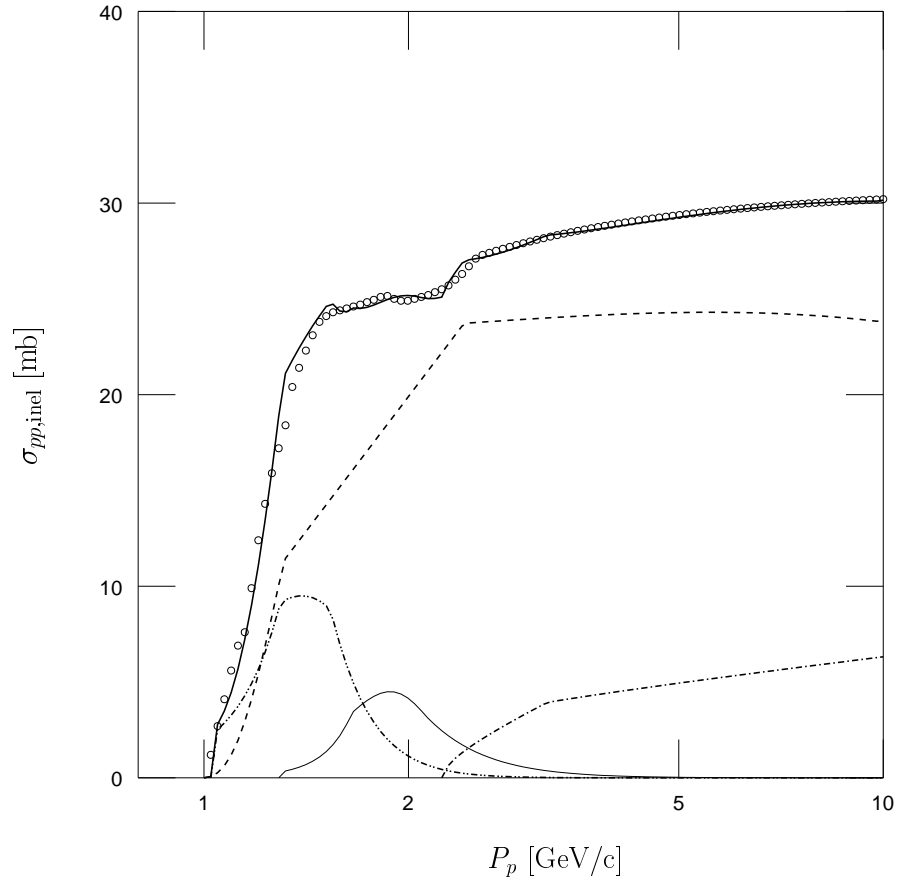
Fig. 2.— Experimental $p - p$ cross sections, as a function of proton momentum, and that of readjusted model A for $T_p < 10$ GeV. Small circles represent the empirical inelastic cross section described in the text. Lines are the same as in Figure 1.

$$\sigma_{\text{NonDiff}}^{pp}(x)[\text{mb}] = \begin{cases} 0 & P_p < 1 \text{ GeV/c}, \\ 0.57(x/a_0)^{1.2}(a_2 + a_3 x^2 + a_4 x^3 \\ \quad +a_5 \exp(-a_6(x+a_7)^2)) & 1 \leq P_p \leq 1.3 \text{ GeV/c}, \\ (b_0|a_1 - x| + b_1|a_0 - x|)/(a_1 - a_0) & 1.3 \leq P_p \leq 2.4 \text{GeV/c}, \\ a_2 + a_3 x^2 + a_4 x^3 \\ \quad +a_5 \exp(-a_6(x+a_7)^2) & 2.4 \leq P_p \leq 10 \text{ GeV/c}, \\ c_0 + c_1 x + c_2 x^2 & P_p > 10 \text{ GeV/c}, \end{cases} \quad (1)$$

$$\sigma_{\text{Diff}}^{pp}(x)[\text{mb}] = \begin{cases} 0 & P_p < 2.25 \text{ GeV/c}, \\ \sqrt{(x-d_0)/d_1} \\ \quad \times(d_2 + d_3 \log_{10}(d_4(x-0.25)) \\ \quad +d_5 x^2 - d_6 x^3) & 2.25 \leq P_p \leq 3.2 \text{ GeV/c}, \\ d_2 + d_3 \log_{10}(d_4(x-0.25)) \\ \quad +d_5 x^2 - d_6 x^3 & 3.2 \leq P_p \leq 100 \text{ GeV/c}, \\ e_0 + e_1 x & P_p > 100 \text{ GeV/c}, \end{cases} \quad (2)$$

$$\sigma_{\Delta 1232}^{pp}(x)[\text{mb}] = \begin{cases} 0 & E_p < 1.4 \text{ GeV}, \\ f_0 E_p^{10} & 1.4 \leq E_p \leq 1.6 \text{ GeV}, \\ f_1 \exp\left(-f_2(E_p - f_3)^2\right) & 1.6 \leq E_p \leq 1.8 \text{ GeV}, \\ f_4 E_p^{-10} & 1.8 \leq E_p \leq 10 \text{ GeV}, \\ 0 & E_p > 10 \text{ GeV}, \end{cases} \quad (3)$$

$$\sigma_{\text{Res}(1600)}^{pp}(x)[\text{mb}] = \begin{cases} 0 & E_p < 1.6 \text{ GeV}, \\ g_0 E_p^{14} & 1.6 \leq E_p \leq 1.9 \text{ GeV}, \\ g_1 \exp\left(-g_2(E_p - g_3)^2\right) & 1.9 \leq E_p \leq 2.3 \text{ GeV}, \\ g_4 E_p^{-6} & 2.3 \leq E_p \leq 20 \text{ GeV}, \\ 0 & E_p > 20 \text{ GeV}, \end{cases} \quad (4)$$

where $x = \log_{10}(P_p[\text{GeV/c}])$ and E_p is the proton energy in GeV.

3.1. Introduction of Resonance-Excitation Processes to Model A

One or both of the projectile and target protons can be excited to baryon resonances in the $p-p$ interaction. Here we use "baryon resonances" to represent both nucleon resonances

(iso-spin=1/2) and Δ resonances (iso-spin=3/2). These excitations enhance the pion production (and hence secondary particle production) near the inelastic threshold. The most prominent resonance among them is $\Delta(1232)$, which has a mass of 1232 MeV/c^2 and decays predominantly ($> 99\%$) to a nucleon and a pion (Hagiwara et al. 2002).

Stecker (1970) proposed a cosmic gamma-ray model in which neutral pions are produced only through the $\Delta(1232)$ excitation for $T_p \leq 2.2$ GeV. The resonance is assumed to move only in the direction of the incident proton. At higher energies, another process, the fireball process, sets in and produces pions with limited transverse momenta.

Dermer (1986a) compared predictions of models on π^0 kinetic energy distribution in the proton-proton center-of-mass (CM) system with experiments and noted that the model by Stecker (1970) reproduces data better than the scaling model by Stephens & Badhwar (1981) for $T_p < 3$ GeV. He proposed a cosmic gamma-ray production model that covers a wider energy range by connecting the two models in the energy range $T_p = 3 - 7$ GeV.

Model A by Kamae et al. (2005) has been constructed primarily for the $p - p$ inelastic interaction $T_p \gg 1$ GeV and has left room for improvement for $T_p < 3$ GeV. The diffraction dissociation component of model A has a resonance-excitation feature similar to that implemented in Stecker (1971) for $T_p > 3$ GeV where either or both protons can be excited to nucleon resonances (iso-spin=1/2 and mass around 1600 MeV/c^2) along the direction of the incident and/or target protons. What has not been implemented in model A is the enhancement by baryon resonances in the inclusive pion production cross sections below $T_p < 3$ GeV.

We note here that the the models by Stecker (1970) and by Dermer (1986a, see also Dermer 1986b) used experimental data on the inclusive π^0 yield (and that of charged pions) to guide their modeling, but not the total inelastic cross section. Model A by Kamae et al. (2005), on the other hand, has simulated all particles in each event (referred to as the "exclusive" particle distribution) for all component cross sections. One exception is simulation of the low-energy non-diffractive process ($T_p < 52.6$ GeV) by Blattnig et al. (2000). The inclusive π^0 (or gamma-ray) yield is obtained by collecting π^0 (or gamma-rays) in simulated exclusive events. When readjusting model A by adding the resonance-excitation feature similar to that by Stecker (1970), overall coherence to model A has been kept. We adjusted the $\Delta(1232)$ excitation cross section to reproduce the total inelastic cross section given in Figure 2 and fixed the average pion multiplicities for $+ : 0 : -$ to those expected by the one-pion-exchange hypothesis, 0.73 : 0.27 : 0.0. As higher-mass resonances begin to contribute, the average pion multiplicity is expected to increase. To reproduce the experimental π^0 inclusive cross section and total inelastic cross section for $T_p < 3$ GeV, we introduced a second resonance, res(1600). This resonance does not correspond to any specific resonance

but represents several baryon resonances at around 1600 MeV/c^2: its pion multiplicities $(+ : 0 : -)$ are assumed to be 1.0:0.8:0.2. We note here that the resonance components favor positive pions significantly over neutral pions while negative pions are strongly suppressed.

The distribution of pion kinetic energy in the $p-p$ center-of-mass (CM) system (T_π) has been adjusted to reproduce the experimental ones given in Figs. 3-5 of Dermer (1986a). For the $\Delta(1232)$ excitation, the probability increases proportionally to T_π up to its maximum, set at $T_\pi = 0.28 \times \mathrm{abs}(T_p - 0.4)^{0.45}$. Here T_π and T_p are measured in GeV/c. The distribution goes to zero beyond this maximum value. For res(1600), the probability distribution increases proportionally to T_π to reach its peak at $T_\pi = 0.16 \times \mathrm{abs}(T_p - 0.4)^{0.45}$. It decreases linearly until reaching zero at twice the peak of T_π.

Pion momentum is directed isotropically in the $p-p$ CM system for res(1600) as well as for $\Delta(1232)$. No angular correlation has been assumed between the two pions from res(1600): this is justified for the astronomical environment where chance of detecting two gamma rays from a same interaction is null. Decay kinematics including the polarization effect has been implemented to the charged pion decay. This treatment allows the resonances to recoil transversely to the direction of the incident proton while the recoil was constrained along the incident proton direction in Stecker (1970).

To validate the resonance components of the readjusted model A, we have compared the model π^0 spectrum in the $p-p$ CM system at $T_p = 0.65$, 0.97, and 2.0 GeV with experimental data in Figures 3, 4, 5. Shown in these figures are contributions of the $\Delta(1232)$, res(1600), non-diffractive, and diffractive processes. Our model reproduces well the shape of pion kinetic energy distribution at $T_p = 0.65$ GeV but begins to concentrate more towards zero kinetic energy than experimental data at $T_p = 0.97$ and 2.0 GeV. Fidelity to the experimental data is much improved when compared with the model by Stephens & Badhwar (1981) but somewhat worse than the one by Stecker (1970) given in Figures 2-6 of Dermer (1986a). The difference among the models becomes less noticeable for pion decay products, gamma-rays, electrons, positrons, and neutrinos.

Our inclusive π^0 cross section, sum of all four components, is compared with experimental data assembled by Stecker (1970) and Dermer (1986a) in Fig. 6. The readjusted model A reproduces experimental data quite well for a wide range of incident proton energy.
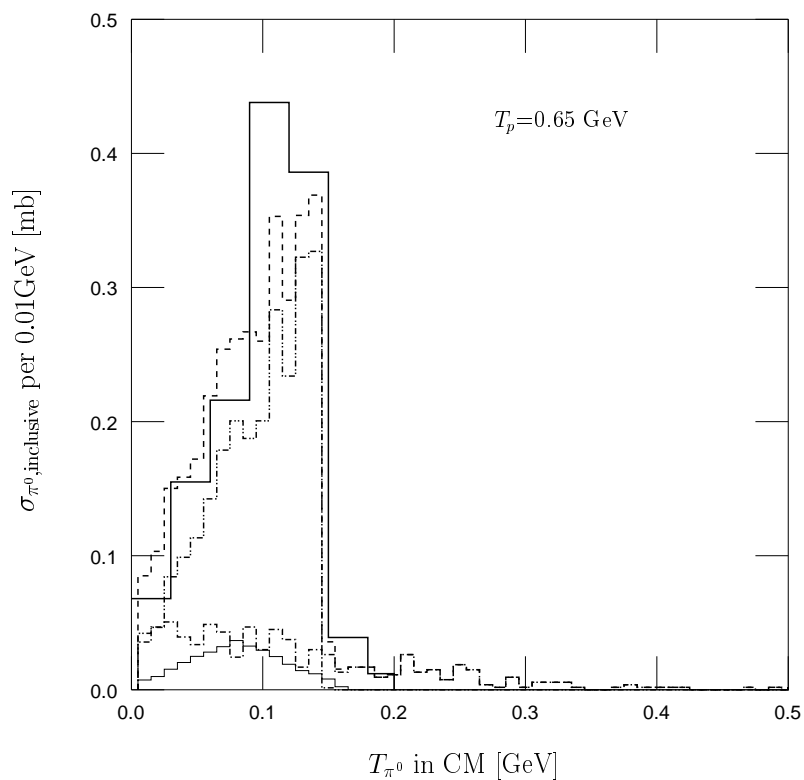
Fig. 3.— Experimental and simulated π^0 kinetic energy distributions in the $p-p$ CM system for $T_p = 0.65$ GeV. The thick solid line is the experimental data taken from Fig. 3 of Dermer (1986a). The dashed line is the sum of all readjusted model A components: non-diffractive (dot-dashed line), $\Delta(1232)$ (double-dot-dashed line), and res(1600) (thin solid line).

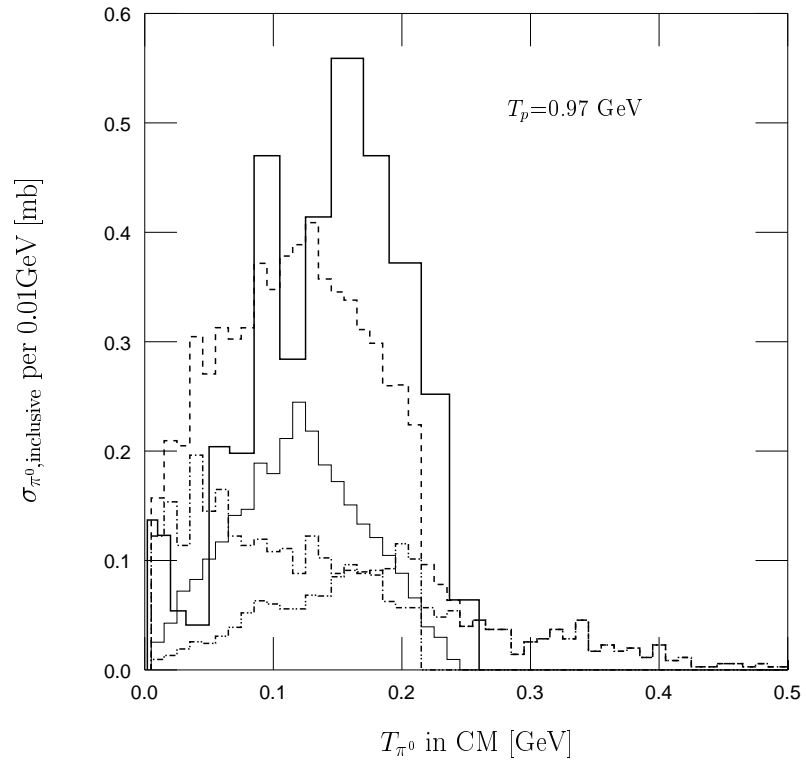Fig. 4.— Experimental and simulated π^0 kinetic energy distributions in the $p-p$ CM system for $T_p = 0.97$ GeV. The thick solid line represents experimental data (taken from Fig. 4 of Dermer (1986a)). Other lines are the same as in Fig. 3.
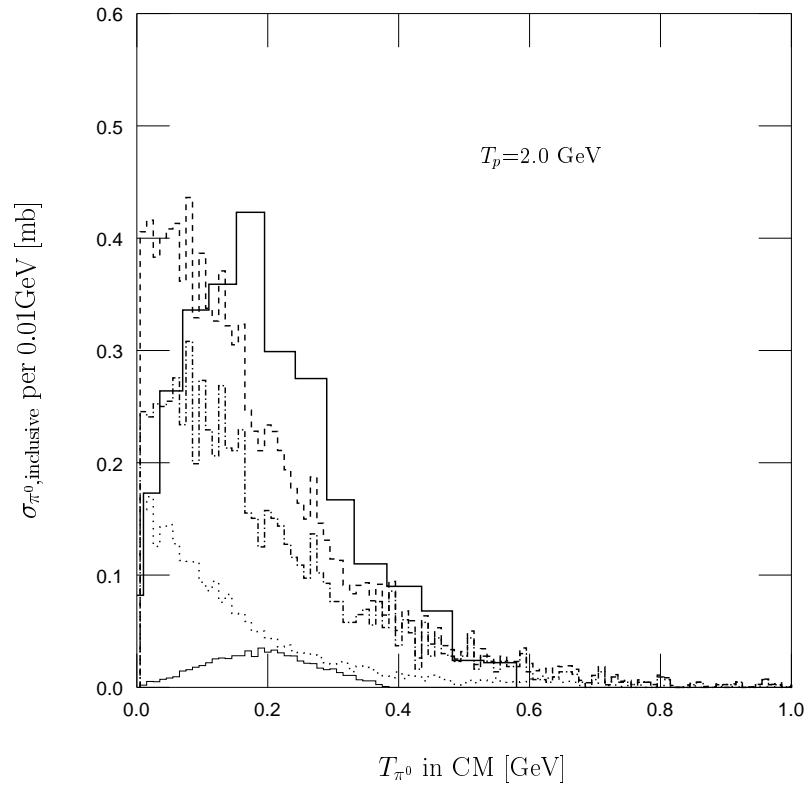
Fig. 5.— Experimental and simulated π^0 kinetic energy distribution in the $p-p$ CM system for $T_p = 2.0$ GeV. the thick solid line represents experimental data (taken from Fig. 5 of Dermer (1986a)), and the dotted line is for the diffractive process. The others are the same as in Fig. 3.

4. Inclusive Spectra of Simulated Events for Mono-Energetic Proton Beam

The first step of parameterization is to generate simulated events for mono-energetic protons. To simplify this step, events have been generated for discrete proton energies at a geometrical series of $T_p = 1000.0 \times 2^{(N-22)/2}$ GeV where $N = 0 - 40$. Each proton kinetic energy (T_p) represents a bin covering between $2^{-0.25}T_p$ and $2^{0.25}T_p$. The sampling density has been increased for $T_p < 1$ GeV by adding points at $T_p = 0.58$ GeV and 0.82 GeV.

Secondary particle spectra are histogrammed from these simulated events in energy bins of width $\Delta E/E = 5$ %. Figures 7a and 7b show thus-obtained inclusive gamma-ray cross sections for the non-diffractive and diffractive processes, for $T_p = 512$ TeV, 8 TeV, 125 GeV and 11.1 GeV respectively. Those for $e^\pm$ are given for $T_p = 8$ TeV and 512 TeV in Figures 8a and 8b.
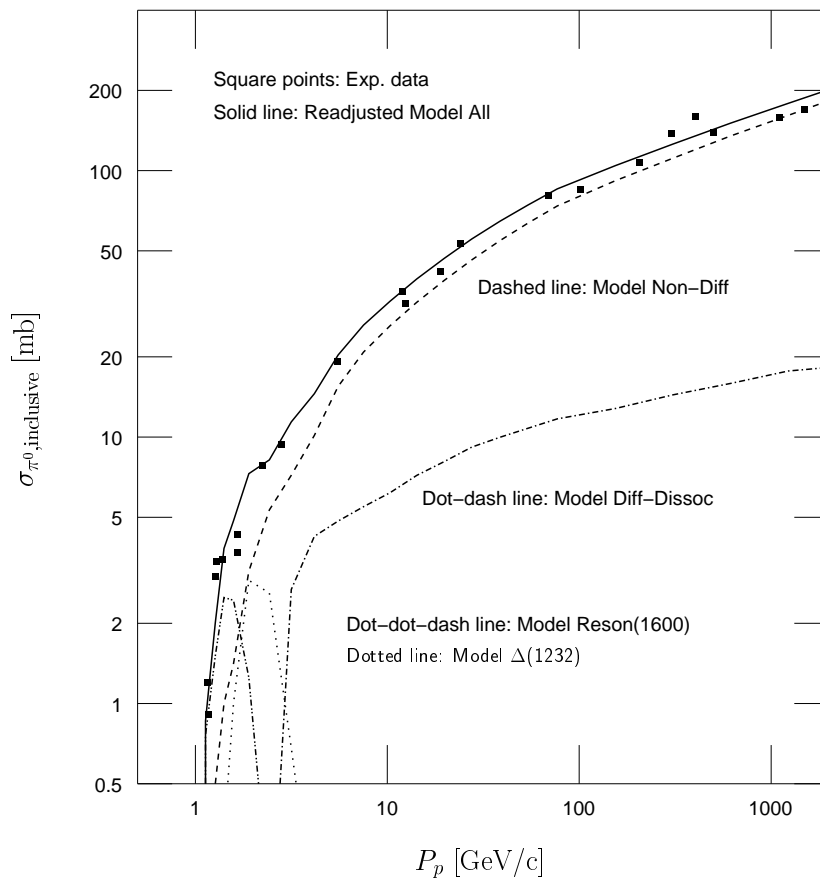
Fig. 6.— Experimental and simulated π^0 inclusive cross section. Experimental data are those assembled by Stecker (1970) and Dermer (1986a). Lines are those of readjusted model A: total (solid line), non-diffractive (dashed line), diffractive process (dot-dashed line), $\Delta(1232)$ (double-dot-dashed line), and res(1600) (dotted line).
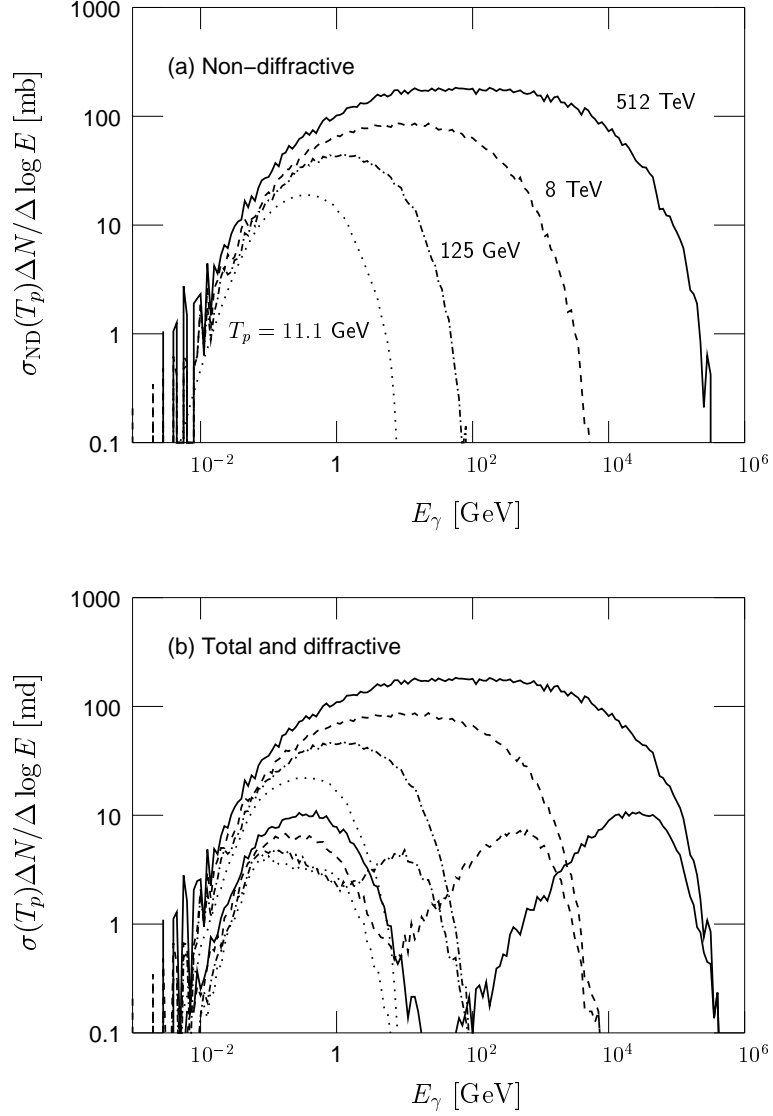
Fig. 7.— Gamma-ray inclusive cross sections by readjusted model A for four mono-energetic protons for (a) the non-diffractive process and (b) the total (top four curves) and the diffractive process (bottom four curves). Note that the diffractive process produces two humps at $T_p = 512$ TeV, 8 TeV and 125 GeV. The four proton kinetic energies are $T_p = 512$ TeV (solid line), 8 TeV (dashed line), 125 GeV (dot-dashed line) and 11.1 GeV (dotted line). The bin width is $\Delta \log(E) = 0.05$. The large fluctuation in the curves at the highest and lowest ends are due to statistics in the simulation.

Fig. 8.— Electron and positron inclusive cross sections by readjusted model A for $T_p = 8$ and 512 TeV for (a) the non-diffractive and (b) diffractive processes. Electron spectra are shown by solid lines and positron spectra by dashed lines. Note that the spectra have two humps in the diffractive process. The bin width is $\Delta\log(E) = 0.05$. The large fluctuation in the histograms at the highest and lowest ends are due to statistics in the simulation.
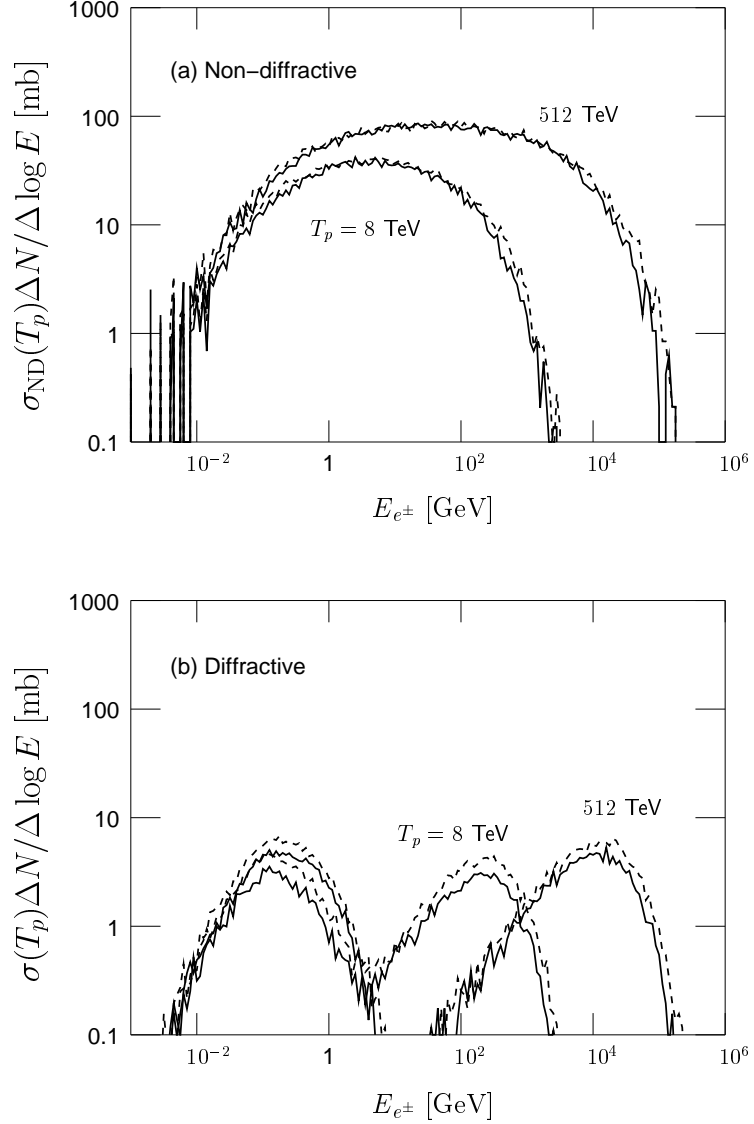
We then define, after several iterations of fitting, functional formulae that reproduce the secondary particle spectra for mono-energetic protons, for the non-diffractive, diffractive, and resonance-excitation processes separately. For the non-diffractive process, the differential inclusive cross section ($\Delta\sigma_{\mathrm{ND}}$) to produce a secondary particle in a bin of width $\Delta E_{\mathrm{sec}}/E_{\mathrm{sec}} = 100\ \%$ centered at E_{sec} is given as

$$\frac{\Delta\sigma_{\mathrm{ND}}(E_{\mathrm{sec}})}{\Delta\log(E_{\mathrm{sec}})} = F_{\mathrm{ND}}(x)F_{\mathrm{ND,kl}}(x), \tag{5}$$

where $E_{\mathrm{sec}}[\mathrm{GeV}]$ is the energy of the secondary particle and $x = \log_{10}(E_{\mathrm{sec}}[\mathrm{GeV}])$. $F_{\mathrm{ND}}(x)$ is the formula representing the non-diffractive cross section, given in equation (6) below, and $F_{\mathrm{ND,kl}}(x)$ is the formula to approximately enforce the energy-momentum conservation limits:

$$
\begin{aligned}
F_{\mathrm{ND}}(x) &= a_0 \exp(-a_1(x - a_3 + a_2(x - a_3)^2)^2) + \\
&\quad a_4 \exp(-a_5(x - a_8 + a_6(x - a_8)^2 + a_7(x - a_8)^3)^2),
\end{aligned} \tag{6}
$$

$$F_{\mathrm{ND,kl}}(x) = \frac{1}{(\exp\left(W_{\mathrm{ND,l}}(L_{\min} - x)\right) + 1)} \frac{1}{(\exp\left(W_{\mathrm{ND,h}}(x - L_{\max})\right) + 1)}, \tag{7}$$

where $L_{\min}$ and $L_{\max}$ are the lower and upper kinematic limits imposed and $W_{\mathrm{ND,l}}$ and $W_{\mathrm{ND,h}}$ are the widths of the kinematic cut-offs; $L_{\min} = -2.6$ for all secondary particles, and the other parameters are listed in Table 2.

For the diffractive process we use a similar function

$$\frac{\Delta\sigma_{\mathrm{diff}}(E_{\mathrm{sec}})}{\Delta\log(E_{\mathrm{sec}})} = F_{\mathrm{diff}}(x)F_{\mathrm{kl}}(x) \tag{8}$$

where $E_{\mathrm{sec}}[\mathrm{GeV}]$ is the energy of the secondary particle and $x = \log_{10}(E_{\mathrm{sec}}[\mathrm{GeV}])$; $F_{\mathrm{diff}}(x)$ represents the diffractive cross section, given in equation (9) below, and $F_{\mathrm{kl}}(x)$ enforces the energy-momentum conservation:

$$
\begin{aligned}
F_{\mathrm{Diff}}(x) &= b_0 \exp(-b_1((x - b_2)/(1 + b_3(x - b_2)))^2) + \\
&\quad b_4 \exp(-b_5((x - b_6)/(1 + b_7(x - b_6)))^2),
\end{aligned} \tag{9}
$$

$$F_{\mathrm{kl}}(x) = \frac{1}{\exp\left(W_{\mathrm{diff}}(x - L_{\mathrm{max}})\right) + 1}, \tag{10}$$

with $W_{\mathrm{diff}} = 75$ and $L_{\mathrm{max}} = \log_{10}(T_p[GeV])$.

For the resonance-excitation processes [$\Delta(1232)$ and res(1600)] we use the function,

$$\frac{\Delta\sigma_{\mathrm{res}}(E_{\mathrm{sec}})}{\Delta\log(E_{\mathrm{sec}})} = F_{\mathrm{res}}(x)F_{\mathrm{kl}}(x), \tag{11}$$

where $E_{\mathrm{sec}}[\mathrm{GeV}]$ is the energy of the secondary particle and $x = \log_{10}(E_{\mathrm{sec}}[\mathrm{GeV}])$, $F_{\mathrm{res}}(x)$ represents the cross section, given in equation (12) below, and $F_{\mathrm{kl}}(x)$, which is the same as for the diffraction process, enforces the energy-momentum conservation:

$$F_{\mathrm{res}}(x) = c_0 \exp\left(-c_1((x - c_2)/(1 + c_3(x - c_2) + c_4(x - c_2)^2))^2\right). \tag{12}$$

To ensure that the parameterized model reproduces the experimental π^0 multiplicity after the readjustment in the resonance-excitation region of T_p, we have renormalized the non-diffractive contribution by multiplying it with a renormalization factor, $r(T_p)$, given below, to the final spectrum. Note that this readjustment does not affected the diffractive process.

$$r(T_p) \simeq 1.01 \quad \text{for} \quad T_p > 1.95\mathrm{GeV}, \tag{13}$$

$$r(y = \log_{10}(T_p)) = 3.05 \exp\left(-107((y + 3.25)/(1 + 8.08(y + 3.25)))^2\right) \quad \text{for} \quad T_p \leq 1.95\mathrm{GeV}. \tag{14}$$

For all other secondary particles, $r(y = \log_{10}(T_p))$ is found in Tables 4-9.

The simulated gamma-ray inclusive cross sections are superimposed with the parameterized ones in Figures 9a and 9b for three mono-energetic protons, for the non-diffractive and diffractive processes and for the resonance-excitation processes in Figure 10. The agreement is generally good except near the higher and lower kinematical limits where we find a difference of about 10-20%.
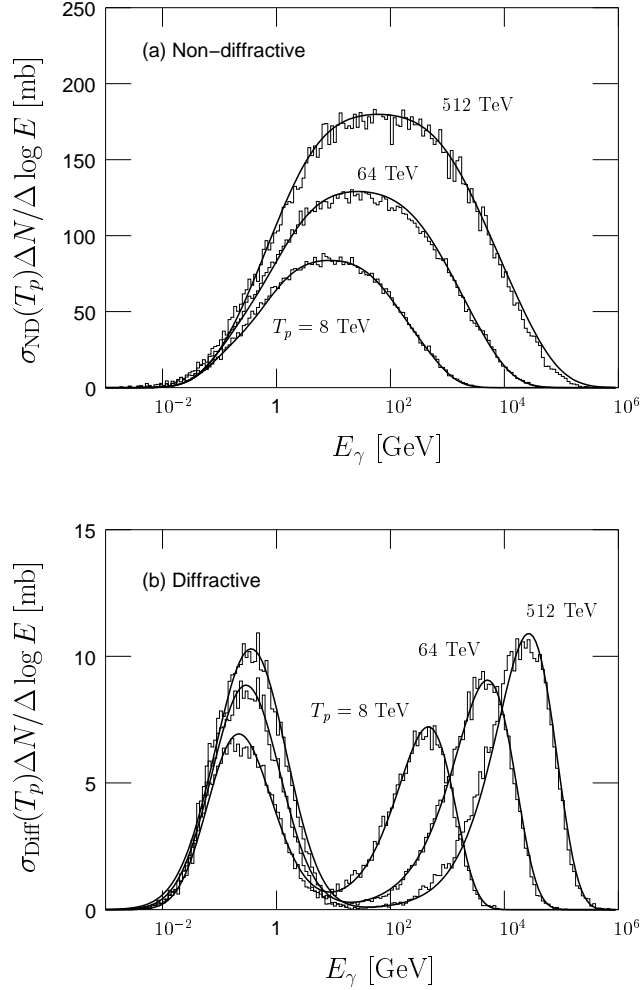
Fig. 9.— Simulated (histograms) and parameterized (solid lines) gamma-ray inclusive cross sections for (a) non-diffractive and (b) diffractive processes for $T_p = 8$, 64 and 512 TeV. The parameterized cross sections are defined by equations (6) and (9), and parameters given in Table 3.

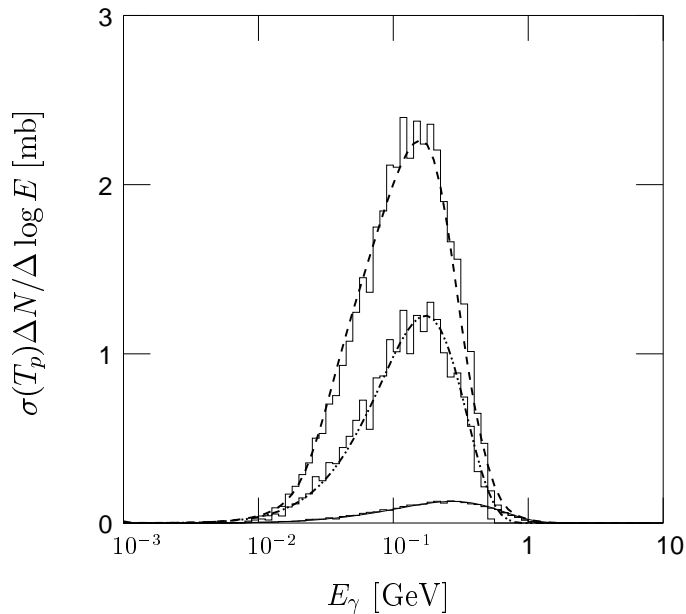Fig. 10.— Simulated (histograms) and parameterized (lines) gamma-ray inclusive cross sections for the resonance-excitation processes at $T_p = 0.69$ GeV. $\Delta(1232)$ (double-dot-dashed line), res(1600) (thin solid line), and the sum of all model distributions (dashed line). The parameterized cross sections are defined by equations (12) for both $\Delta(1232)$ and res(1600), and parameters are given in Table 3.

5.   Representation of Parameters as Functions of Incident Proton Energy

The parameterization formulae for secondary particles for mono-energetic protons (equations [6], [9] and [12]) have nine, eight, and five parameters for each T_p for non-diffractive, diffractive, and resonance-excitation processes respectively. These parameters depend on the proton kinetic energy, T_p. The final step of the parameterization is to find simple functions representing energy dependence of these parameters. Functions obtained by fitting often give values different significantly from those found for mono-energetic protons near the kinematic limits and produce artifacts in the wide range spectral energy density, as described previously. Some manual adjustments have been made to control possible artifacts.

5.1.   Parameterized Gamma Ray Spectrum

The final functional representation of inclusive cross sections for secondary gamma-rays is given in equations (6), (9), and (12) with parameters defined as functions of T_p in TeV (not GeV) in Table 3. The total inclusive gamma-ray spectrum is the sum of the non-diffractive, diffractive, and resonance-excitation contributions. The spectrum produced by protons with a continuous spectrum can be calculated by summing over the total gamma-ray spectra for mono-energetic protons with appropriate spectral weight. For example, the spectra for power-law protons extending to $T_p = 512$ TeV with index=2 and index=2.7 have been calculated and compared with the corresponding histograms produced from the simulated events in Figure 11. The parameterized model reproduces either spectrum within 10%: it predicts 10-20% more gamma-rays than simulation by the readjusted model A at the higher kinematical limit.
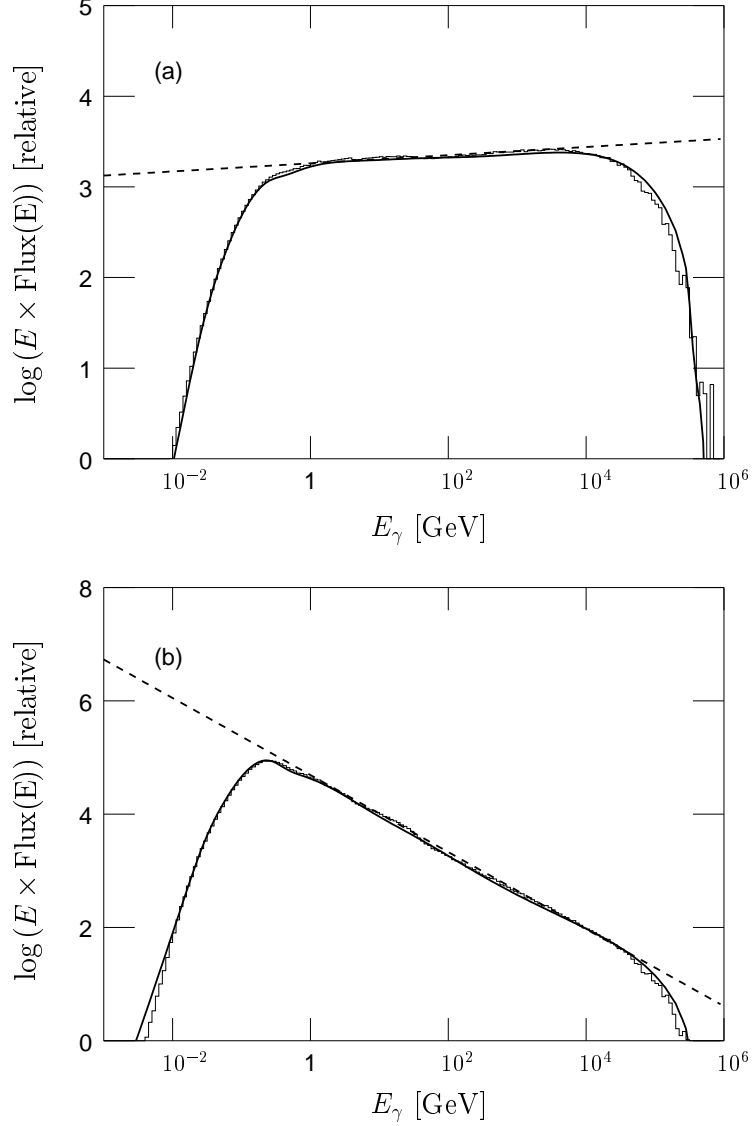
Fig. 11.— Gamma-ray spectra produced by protons with power-law spectrum cutoff at $T_p = 512$ TeV: (a) index=2 and (b) index=2.7 by the parametrized model (*solid lines*) defined by equations (6), (9), (12), and by Table 3. The histograms are those of the simulation by the readjusted model A. The dashed straight line corresponds to an index of (a) 1.95 and (b) 2.68.

5.2.   Parameterized $e^\pm$ and Neutrino Spectra

The parameterization has been extended to other secondary particles, e^-, e^+, ν_e, $\bar{\nu}_e$, ν_μ, and $\bar{\nu}_\mu$, in the same way as for gamma-rays. Their functional formulae are represented by equations (6), (9), and (12) with the parameters defined in Tables 4, 5, 6, 7, 8, and 9, respectively. We note that no π^- is produced in $\Delta(1232)$ decay in readjusted model A and, hence, no e^- and $\bar{\nu}_e$ either.

We note that the secondary electron and positron spectra from charged pion and muon decays have been calculated including the polarization effect of the weak interaction theory. The spectra produced by power-law protons of index=2.0 and 2.7 ($T_p < 512$ TeV) have been computed based on these parameterized models in Figure 12 for $e^\pm$ and Figure 13 for ν_μ. We note in Figure 12 that more e^+ are produced than e^- throughout their spectra. This is largely due to the charge conservation and enhanced by the fact that we have neglected α-particles and neutron decays. The number of electrons produced in the $p - p$ interaction will match that of positrons if we include electrons coming out of neutron decays.

For given T_p, electrons from neutron decays have low energy (mostly with $E < 10$ MeV) as shown by the lower histograms in Figure 12. They do not contribute to the high energy gamma-ray spectrum.
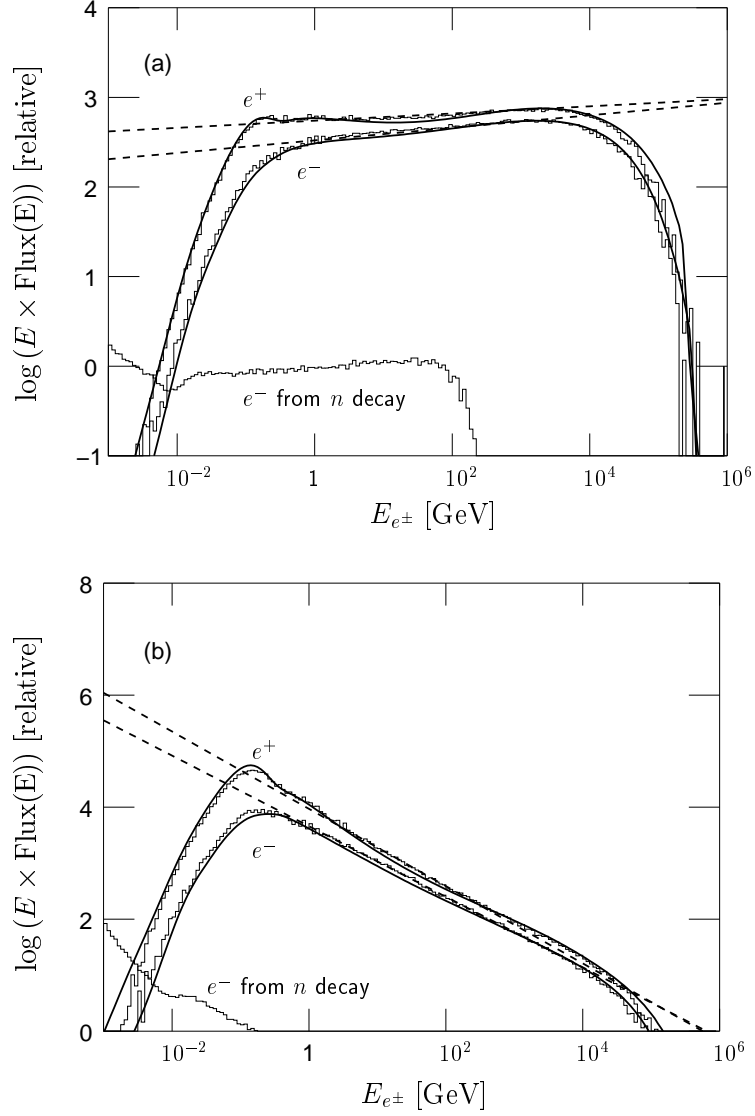
Fig. 12.— Electron and positron spectra produced by protons with power-law spectrum cutoff at $T_p = 512$ TeV: (a) index=2 and (b) index=2.7 by the readjusted model A and by the parameterized model (solid lines) defined by equations (6), (9), and (12). The parameters are defined in Table 4 for electrons and in Table 5 for positrons. The histograms are those of the simulation by the readjusted model A. The dashed straight lines correspond to asymptotic power-laws: for electrons 1.93 and 2.63 respectively; and for positrons 1.96 and 2.69 respectively. The histograms in the lower left corner of (a) and (b) show the spectra of the electrons from the neutrons produced by the power-law protons.
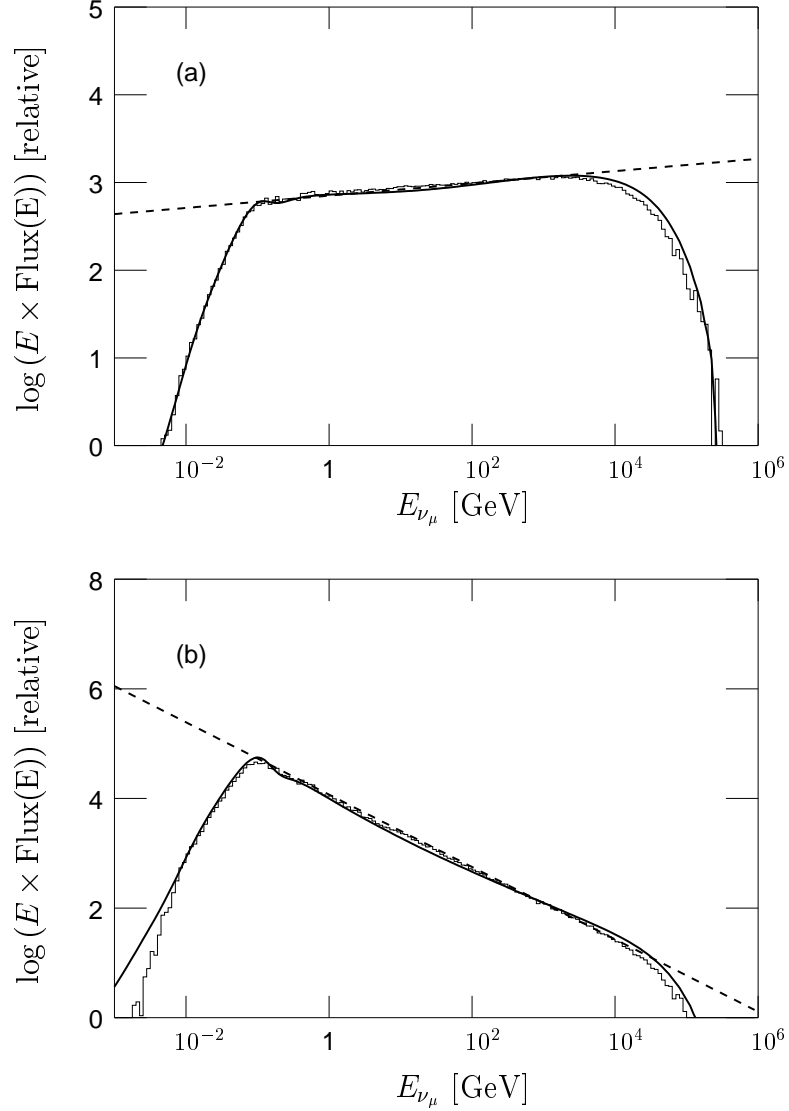
Fig. 13.— Muon neutrino spectra produced by protons with power-law spectrum of (a) index=2 and (b) index=2.7 by the parameterized model (solid curves) defined by equations (6), (9), and (12). The parameters are defined in Table 8. The histograms are those of the simulation by model A and Δ-excitation. The dashed straight lines correspond to index of (a) 1.93 and (b) 2.66. Note that the muon antineutrino spectra are the same.
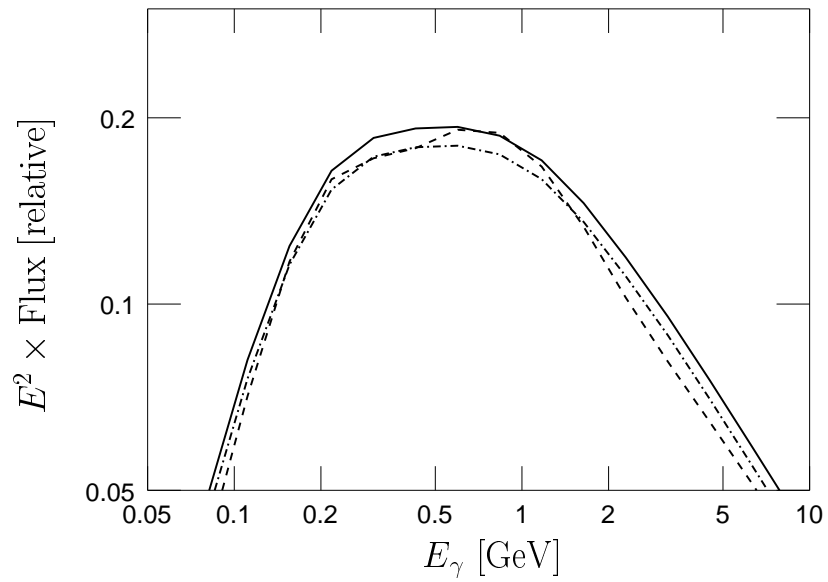
Fig. 14.— The π^0 gamma-ray spectra in the Galactic ridge obtained with Galprop with the parameter set, galdef 500180: the Galprop built-in $p - p$ interaction model (dashed line); the present parameterized $p - p$ interaction model (dash-dot line); the present parameterized model normalized to the dashed line in the energy band 0.7-0.8 GeV (solid line).

6. Application to Galactic Diffuse Gamma-Ray Emission

We have replaced the π^0 production subroutine of Galprop (Strong & Moskalenko 1997, 2001) with the present parameterized model and compared the Galactic diffuse gamma-ray spectra of π^0 origin with that by the built-in subroutine. A common parameter set, galdef 500180 described in Strong et al. (2004), has been used in the two calculations.

As shown in Figure 14, the present parameterized model gives a flatter and smoother spectral energy distribution between $E_\gamma = 0.3 - 2$ GeV, smaller gamma-ray yield between $0.5 - 1.3$ GeV, and a higher power-law index between $1 - 5$ GeV than the Galprop built-in model. In Kamae et al. (2005), gamma-ray spectrum of the Galprop built-in model was compared with that of model A, after being normalized in the energy range $E < 300$ MeV. This normalization enhanced gamma-ray yield in the GeV range relative to sub-GeV range. The Galprop built-in $p-p$ interaction model has been tuned to reproduce accelerator experiments better than model A of Kamae et al. (2005) near the threshold. We have included the resonance contributions in the present model to improve this shortcoming near the threshold. Hence we have change the normalization point to the peak region in $E^2 d\mathrm{flux}/dE$, $E_\gamma = 0.7 - 0.8$ GeV, where gamma-rays from π^0 decays are expected to dominate (see Figure 14, dashed curve). The present model thus normalized gives $\sim 20\%$ higher gamma-ray yield than Galprop at 2 GeV: this is substantially lower than the difference (about 50%) shown in Figure 7 of Kamae et al. (2005). The gamma-ray power-law index of the present model is harder by about 0.05 than that by the Galprop built-in model, just as the model A of Kamae et al. (2005) predicts.

7. Conclusion and Future Prospects

We have presented the inclusive cross sections of stable secondary particles (γ, $e^\pm$, ν_e, $\bar{\nu}_e$, ν_μ, and $\bar{\nu}_\mu$) produced by the $p-p$ interaction in parameterized formulae. They facilitates computation of secondary particle spectra for arbitrary proton spectra as shown for Galactic diffuse gamma-ray spectrum (Figure 14). Various effects that these secondary particles may have in astronomical environments can also be calculated at a higher precision. The formulae incorporate all important known features of the $p-p$ interaction up to about $T_p = 500$ TeV and hence will also be useful in calculating background when searching for new phenomena.

The parameterized model predicts all secondary particle spectra to have harder power-law indices than that of the incident proton and their inclusive cross sections to be larger than those expected from the old $p-p$ interaction models. When used to replace the $p-p$ subroutine in Galprop (Strong & Moskalenko 1997, 2001), the model gives a flatter spectral

energy density distribution between $0.3-5$ GeV. The absolute gamma-ray yield predicted by the model is smaller than that by the Galprop model for $E_\gamma < 1.5$ GeV but higher for $E_\gamma > 1.5$ GeV. If normalized near the peak in $E^2 d\text{flux}/dE$ ($E_\gamma = 0.7-0.8$ GeV), the parameterized model gives $\sim 20\%$ higher gamma-ray yield at 2 GeV than the model of Galprop: our model with this normalization can account for $\sim 20\%$, not $\sim 50\%$ as was claimed in Kamae et al. (2005), of the discrepancy between the diffuse Galactic Ridge gamma-ray spectrum observed by EGRET and model predictions for the proton spectrum near the solar system (the power-law index ~ 2.7) (Hunter et al. 1997). We note the discrepancy will be reduced by inclusion of the inverse Compton component (see, for example, a model by Strong et al. (2004)).

The present model also predicts more e^+ than e^- at energies higher wherever those produced by $p-p$ interaction become comparable in flux to primary e^- and e^+. The formulae and parameters given in the appendices are available as supplementary on-line material both in C language format and as C subroutine. We are currently parametrizing the angular distribution of gamma-rays relative to the incident proton direction. The results will be published elsewhere.

8. Acknowledgments

REFERENCES

Aharonian, F. A., 2004, "Very High Energy Cosmic Gamma Radiation: A Crucial Window on the Extreme Universe" (World Scientific Publishing)

Aharonian, F. A., 2005, Science, 307, 1938: available as astro-ph/0504380

Aharonian, F. A., et al., 2004b, Nature, 432, 75: available as astro-ph/0411533

Aharonian, F. A., et al., 2004c, A&A, 425, L13: available as astro-ph/0408145

Aharonian, F. A., Völk , Horns, D. 2004, Proc. Int. Symp. on High Energy Gamma-Ray Astronomy (World Scientific)

Berezhko, E. G. & Völk, H. J., 2000, ApJ, 540, 923

Blattnig, S. R., et al. 2000, Phys. Rev., D62, 094030

Bloemen, J.B.G.M., et al. 1984, A&A, 135, 12

Bloemen, J.B.G.M. 1985, A&A, 145, 391

Böttcher, M. and Reimer, A. 2004 ApJ 609, 576

Crawford, J. F. et al. 1980 Phys. Rev. C22, 1184

Dermer, C. D. 1986a, A&A, 157, 223

Dermer, C. D. 1986b, ApJ, 307, 47

DuVernois, M.A., et al. 2001, ApJ 559, 296

Enomoto, R., et al., 2002, Nature, 416, 823: available as astro-ph/0204422

Field, R.D. 2002, Matrix Element and Monte Carlo Tuning Workshop,
    `http://cepa.fnal.gov/CPD/MCTuning`, `http://www.phys.ufl.edu/~rfield/cdf`

Hagiwara, K., et al. 2002, Phys. Rev., D66, 010001.

Halzen, F., in Aharonian, F. A., Völk, H. J., and Horns, D. (eds.) Proc. Second Int. Symposium on High Energy Gamma-Ray Astronomy (July 2004, Heidelberg) p.3

Hayakawa, S. 1969, "Cosmic Ray Physics" (John-Wiley)

Hunter, S.D., et al. 1997, ApJ, 481, 205

Iyudin, A. F., et al. 2005, A&A 429, 225

Kamae, T., Abe., T, & Koi, T., 2005, ApJ 620, 244

Katagiri, H., et al., 2005, ApJ, 619, L163: available as astro-ph/0412623

Koyama, K., et al. 1997, PASJ 49, L7

Mårtensson, J., et al. 2000 Phys. Rev. C62, 014610

Mayer-Hasselwander, H.A., et al. 1982, A&A, 105, 164

Mori, M. 1997, ApJ, 478, 225

Mücke, A., and Protheroe, R. J. 2001, Astroparticle Physics 15, 121

Mücke, A., et al. 2003, Astroparticle Physics 18, 593

Müller, D. 2001, Adv. Space Res. 27, 659

Murthy, P.V.R. and Wolfendale, A. W. 1986, "Gamma-ray Astronomy" (Cambridge University Press)

Ong, R. A., 1998, Physics Reports, 305, 93

PAMELA Collaboration, see `http://wizard.roma2.infn.it/pamela`

Schönfelder, V. (ed) 2001, "The Universe in Gamma Rays" (Springer-Verlag)

Schlickeiser, R. 2002, "Cosmic Ray Astrophysics", Springer Verlag

Sjöstrand, T., Lonnblad, L., and Mrenna, S. 2001, "Pythia 6.2: Physics and Manual", hep-ph/0108264

Sjöstrand, T., and Skands, P. Z. 2004, hep-ph/0402078

Slane, P., et al. 1999, ApJ 525, 357

Stanev, T., 2004, "High Energy Cosmic Rays" (Springer Verlag)

Stecker, F. 1970, Astrophys. & Space Science, 377

Stecker, F. 1971, "Cosmic Gamma Rays" NASA SP-249 (NASA Scientific and Technical Information Office)

Stecker, F. 1973, ApJ, 185, 499

Stecker, F. 1990, in Shapiro, M.M., and Wefel, J.P. (eds.), "Cosmic Gamma Rays, Neutrinos and Related Astrophysics", p.89

Stephens, S.A., and Badhwar, G.D. 1981, Astrophys. Space Sci, 76, 213

Stephens, S.A. 2001, Adv. Space Res. 27, 687

Strong, A.W., et al. 1978, MNRAS, 182, 751

Strong, A.W., et al. 1982, A&A, 115, 404

Strong, A.W., and Moskalenko, I.V. 1997, Proc. Fourth Compton Symp., (eds) Dermer, C. D., Strickman, M. S., and Kurfess, J. D., p.1162; astro-ph/9709211

Strong, A. W., and Moskalenko, I. V. 2001, Proc. of 27th ICRC 2001 (Hamburg), p.1942 and astro-ph/0106504

Strong, A. W., Moskalenko, I. V., and Reimer, O. 2000, ApJ, 537, 763; Errortum: 2000, ibid, 541, 1109

Strong, A. W., Moskalenko, I. V., and Reimer, O. 2004, ApJ, 613, 962

Tsunemi, H., et al. 2000, PASJ 52, 887

Uchiyama, Y, Aharonian, F. A., and Takahashi, T. 2003, A&A 400, 567

Weekes, T. C., 2003, Proc. 28th Int. Cosmic Ray Conf. (Aug. 2003, Tsukuba): available as astro-ph/0312179

Table 1: Constants for equations 1, 2, 3 and 4.

$a_0 = 0.1176$	$b_0 = 11.34$	$c_0 = 28.5$	$d_0 = 0.3522$	$e_0 = 5.922$	$f_0 = 0.0834$	$g_0 = 0.0004257$
$a_1 = 0.3829$	$b_1 = 23.72$	$c_1 = -6.133$	$d_0 = 0.1530$	$e_1 = 1.632$	$f_1 = 9.5$	$g_1 = 4.5$
$a_2 = 23.10$		$c_2 = 1.464$	$d_2 = 1.498$		$f_2 = -5.5$	$g_2 = -7.0$
$a_3 = 6.454$			$d_3 = 2.0$		$f_3 = 1.68$	$g_3 = 2.1$
$a_4 = -5.764$			$d_4 = 30.0$		$f_4 = 3134$	$g_4 = 503.5$
$a_5 = -23.63$			$d_5 = 3.155$			
$a_6 = 94.75$			$d_6 = 1.042$			
$a_7 = 0.02667$						

Table 2: Kinematic limit parameters for the non-diffractive process. Proton kinetic energy T_p is in GeV.

Particle	$L_{\max}$	$W_{\mathrm{ND,l}}$	$W_{\mathrm{ND,h}}$
γ	$0.96\log_{10}(T_p)$	15	44
e^-	$0.96\log_{10}(T_p)$	20	45
e^+	$0.94\log_{10}(T_p)$	15	47
ν_e	$0.98\log_{10}(T_p)$	15	42
$\bar{\nu}_e$	$0.98\log_{10}(T_p)$	15	40
ν_μ	$0.94\log_{10}(T_p)$	20	45
$\bar{\nu}_\mu$	$0.98\log_{10}(T_p)$	15	40

Table 3: Parameters describing gamma-ray spectra for arbitrary proton energy.

Parameter	Formulae as functions of the proton kinetic energy ($y = \log_{10}(T_p)$) in TeV.
Non-diff., equation 6	
a_0	$-0.51187(y + 3.3) + 7.6179(y + 3.3)^2 - 2.1332(y + 3.3)^3 + 0.22184(y + 3.3)^4$
a_1	$-1.2592 \cdot 10^{-5} + 1.4439 \cdot 10^{-5} \exp\left(-0.29360(y + 3.4)\right) + 5.9363 \cdot 10^{-5}/(y + 4.1485) + 2.2640 \cdot 10^{-6}y - 3.3723 \cdot 10^{-7}y^2$
a_2	$-174.83 + 152.78 \log_{10}\left(1.5682(y + 3.4)\right) - 808.74/(y + 4.6157)$
a_3	$0.81177 + 0.56385y + 0.0040031y^2 - 0.0057658y^3 + 0.00012057y^4$
a_4	$0.68631(y + 3.32) + 10.145(y + 3.32)^2 - 4.6176(y + 3.32)^3 + 0.86824(y + 3.32)^4 - 0.053741(y + 3.32)^5$
a_5	$9.0466 \cdot 10^{-7} + 1.4539 \cdot 10^{-6} \log_{10}\left(0.015204(y + 3.4)\right) + 1.3253 \cdot 10^{-4}/(y + 4.7171)^2 - 4.1228 \cdot 10^{-7}y + 2.2036 \cdot 10^{-7}y^2$
a_6	$-339.45 + 618.73 \log_{10}\left(0.31595(y + 3.9)\right) + 250.20/(y + 4.4395)^2$
a_7	$-35.105 + 36.167y - 9.3575y^2 + 0.33717y^3$
a_8	$0.17554 + 0.37300y - 0.014938y^2 + 0.0032314y^3 + 0.0025579y^4$
$r(y)$	$3.05 \exp\left(-107((y + 3.25)/(1 + 8.08(y + 3.25)))^2\right)$ for $T_p \leq 1.95$ GeV
	1.01 for $T_p > 1.95$ GeV
Diffraction, equation 9	
b_0	$60.142 \tanh\left(-0.37555(y + 2.2)\right) - 5.9564(y + 0.59913)^2 + 6.0162 \cdot 10^{-3}(y + 9.4773)^4$
b_1	$35.322 + 3.8026 \tanh\left(-2.5979(y + 1.9)\right) - 2.1870 \cdot 10^{-4}(y + 369.13)^2$
b_2	$-15.732 - 0.082064 \tanh\left(-1.9621(y + 2.1)\right) + 2.3355 \cdot 10^{-4}(y + 252.43)^2$
b_3	$-0.086827 + 0.37646 \exp\left(-0.53053((y + 1.0444)/(1.0 + 0.27437(y + 1.0444)))^2\right)$
	Important: $b_0, \ldots, b_3 = 0$ for $T_p < 5.52$ GeV
b_4	$2.5982 + 0.39131(y + 2.95)^2 - 0.0049693(y + 2.95)^4 + 0.94131 \exp\left(-24.347(y + 2.45 - 0.19717(y + 2.45)^2)^2\right)$
b_5	$0.11198 - 0.64582y + 0.16114y^2 + 2.2853 \exp\left(-0.0032432((y - 0.83562)/(1.0 + 0.33933(y - 0.83562)))^2\right)$
b_6	$1.7843 + 0.91914y + 0.050118y^2 + 0.038096y^3 - 0.027334y^4 - 0.0035556y^5 + 0.0025742y^6$
b_7	$-0.19870 - 0.071003y + 0.019328y^2 - 0.28321 \exp\left(-6.0516(y + 1.8441)^2\right)$
$\Delta(1232)$, equation 12	
c_0	$2.4316 \exp\left(-69.484((y + 3.1301)/(1.0 + 1.24921(y + 3.1301)))^2\right) - 6.3003 - 9.5349/y + 0.38121y^2$
c_1	$56.872 + 40.627y + 7.7528y^2$
c_2	$-5.4918 - 6.7872 \tanh\left(4.7128(y + 2.1)\right) + 0.68048y$
c_3	$-0.36414 + 0.039777y$
c_4	$-0.72807 - 0.48828y - 0.092876y^2$
Res1600), equation 12	
d_0	$3.2433 \exp\left(-57.133((y + 2.9507)/(1.0 + 1.2912(y + 2.9507)))^2\right) - 1.0640 - 0.43925y$
d_1	$16.901 + 5.9539y - 2.1257y^2 - 0.92057y^3$
d_2	$-6.6638 - 7.5010 \tanh\left(30.322(y + 2.1)\right) + 0.54662y$
d_3	$-1.50648 - 0.87211y - 0.17097y^2$
d_4	$0.42795 + 0.55136y + 0.20707y^2 + 0.027552y^3$

Table 4: Parameter describing electron spectra for arbitrary proton energy.

Parameters	Formulae as functions of the proton kinetic energy ($y = \log_{10}(T_p)$) in TeV.
Non-diff., equation 6	
a_0	$-0.018639(y+3.3) + 2.4315(y+3.3)^2 - 0.57719(y+3.3)^3 + 0.063435(y+3.3)^4$
a_1	$7.1827 \cdot 10^{-6} - 3.5067 \cdot 10^{-6}y + 1.3264 \cdot 10^{-6}y^2 - 3.3481 \cdot 10^{-7}y^3 + 2.3551 \cdot 10^{-8}y^4 + 3.4297 \cdot 10^{-8}y^5$
a_2	$563.91 - 362.18 \log_{10}(2.7187(y+3.4)) - 2.8924 \cdot 10^4/(y+7.9031)^2$
a_3	$0.52684 + 0.57717y + 0.0045336y^2 - 0.0089066y^3$
a_4	$0.36108(y+3.32) + 1.6963(y+3.32)^2 - 0.074456(y+3.32)^3 - 0.071455(y+3.32)^4 + 0.010473(y+3.32)^5$
a_5	$9.7387 \cdot 10^{-5} + 7.8573 \cdot 10^{-5} \log_{10}(0.0036055(y+4.3)) + 0.00024660/(y+4.9390) - 3.8097 \cdot 10^{-7}y^2$
a_6	$-273.00 - 106.22 \log_{10}(0.34100(y+3.4)) + 89.037y - 12.546y^2$
a_7	$432.53 - 883.99 \log_{10}(0.19737(y+3.9)) - 4.1938 \cdot 10^4/(y+8.5518)^2$
a_8	$-0.12756 + 0.43478y - 0.0027797y^2 - 0.0083074y^3$
$r(y)$	$3.63 \exp(-106((y+3.26)/(1+9.21(y+3.26)))^2) - 0.182y - 0.175y^2$ for $T_p \leq 15.6$ GeV
	1.01 for $T_p > 15.6$ GeV
Diffraction, equation 9	
b_0	$0.20463 \tanh(-6.2370(y+2.2)) - 0.16362(y+1.6878)^2 + 3.5183 \cdot 10^{-4}(y+9.6400)^4$
b_1	$1.6537 + 3.8530 \exp(-3.2027((y+2.0154)/(1.0+0.62779(y+2.0154)))^2)$
b_2	$-10.722 - 0.082672 \tanh(-1.8879(y+2.1)) + 1.4895 \cdot 10^{-4}(y+256.63)^2$
b_3	$-0.023752 - 0.51734 \exp(-3.3087((y+1.9877)/(1.0+0.40300(y+1.9877)))^2)$
	Important: $b_0, \ldots, b_3 = 0$ for $T_p < 5.52$ GeV
b_4	$0.94921 + 0.12280(y+2.9)^2 - 7.1585 \cdot 10^{-4}(y+2.9)^4 + 0.52130 \log_{10}(y+2.9)$
b_5	$-4.2295 - 1.0025 \tanh(9.0733(y+1.9)) - 0.11452 * (y-62.382)$
b_6	$1.4862 + 0.99544y - 0.042763y^2 - 0.0040065y^3 + 0.0057987y^4$
b_7	$6.2629 + 6.9517 \tanh(-0.36480(y+2.1)) - 0.026033 * (y-2.8542)$
Res1600), equation 12	
d_0	$0.37790 \exp(-56.826((y+2.9537)/(1.0+1.5221(y+2.9537)))^2) - 0.059458 + 0.0096583y^2$
d_1	$-5.5135 - 3.3988y$
d_2	$-7.1209 - 7.1850 \tanh(30.801(y+2.1)) + 0.35108y$
d_3	$-6.7841 - 4.8385y - 0.91523y^2$
d_4	$-134.03 - 139.63y - 48.316y^2 - 5.5526y^3$

Table 5: Parameters describing positron spectra for arbitrary proton energy.

Parameters	Formulae as functions of the proton kinetic energy $(y = \log_{10}(T_p))$ in TeV.
Non-diff., equation 6	
a_0	$-0.79606(y+3.3) + 7.7496(y+3.3)^2 - 3.9326(y+3.3)^3 + 0.80202(y+3.3)^4 - 0.054994(y+3.3)^5$
a_1	$6.7943 \cdot 10^{-6} - 3.5345 \cdot 10^{-6}y + 6.0927 \cdot 10^{-7}y^2 + 2.0219 \cdot 10^{-7}y^3 + 5.1005 \cdot 10^{-8}y^4 - 4.2622 \cdot 10^{-8}y^5$
a_2	$44.827 - 81.378 \log_{10}(0.027733(y+3.5)) - 1.3886 \cdot 10^4/(y+8.4417)$
a_3	$0.52010 + 0.59336y + 0.012032y^2 - 0.0064242y^3$
a_4	$2.1361(y+3.32) + 1.8514(y+3.32)^2 - 0.47872(y+3.32)^3 + 0.0032043(y+3.32)^4 + 0.0082955(y+3.32)^5$
a_5	$1.0845 \cdot 10^{-6} + 1.4336 \cdot 10^{-6} \log_{10}(0.0077255(y+4.3)) + 1.3018 \cdot 10^{-4}/(y+4.8188)^2 + 9.3601 \cdot 10^{-8}y$
a_6	$-267.74 + 14.175 \log_{10}(0.35391(y+3.4)) + 64.669/(y-7.7036)^2$
a_7	$138.26 - 539.84 \log_{10}(0.12467(y+3.9)) - 1.9869 \cdot 10^4/(y+7.6884)^2 + 1.0675y^2$
a_8	$-0.14707 + 0.40135y + 0.0039899y^2 - 0.0016602y^3$
$r(y)$	$2.22 \exp\left(-98.9((y+3.25)/(1+10.4(y+3.25)))^2\right)$ for $T_p \le 5.52$ GeV
	1.0 for $T_p > 5.52$ GeV
Diffraction, equation 9	
b_0	$29.192 \tanh(-0.37879(y+2.2)) - 3.2196(y+0.67500)^2 + 0.0036687(y+9.0824)^4$
b_1	$-142.97 + 147.86 \exp\left(-0.37194((y+1.8781)/(1.0+3.8389(y+1.8781)))^2\right)$
b_2	$-14.487 - 4.2223 \tanh(-13.546(y+2.2)) + 1.6988 \cdot 10^{-4}(y+234.65)^2$
b_3	$-0.0036974 - 0.41976 \exp\left(-6.1527((y+1.8194)/(1.0+0.99946(y+1.8194)))^2\right)$
	Important: $b_0, \ldots, b_3 = 0$ for $T_p < 11.05$ GeV
b_4	$1.8108 + 0.18545(y+2.9)^2 - 0.0020049(y+2.9)^4 + 0.85084 \exp\left(-14.987(x+2.29-0.18967(x+2.29)^2)^2\right)$
b_5	$2.0404 - 0.51548 \tanh(2.2758(y+1.9)) - 0.035009/(y-6.6555)$
b_6	$1.5258 + 1.0132y - 0.064388y^2 - 0.0040209y^3 - 0.0082772y^4$
b_7	$3.0551 + 3.5240 \tanh(-0.36739(y+2.1)) - 0.13382*(y-2.7718)$
$\Delta(1232)$, equation 12	
c_0	$2.9841 \exp\left(-67.857((y+3.1272)/(1.0+0.22831(y+3.1272)))^2\right) - 6.5855 - 9.6984/y + 0.41256y^2$
c_1	$6.8276 + 5.2236y + 1.4630y^2$
c_2	$-6.0291 - 6.4581 \tanh(5.0830(y+2.1)) + 0.46352y$
c_3	$0.59300 + 0.36093y$
c_4	$0.77368 + 0.44776y + 0.056409y^2$
Res1600), equation 12	
d_0	$1.9186 \exp\left(-56.544((y+2.9485)/(1.0+1.2892(y+2.9485)))^2\right) - 0.23720 + 0.041315y^2$
d_1	$-4.9866 - 3.1435y$
d_2	$-7.0550 - 7.2165 \tanh(31.033(y+2.1)) + 0.38541y$
d_3	$-2.8915 - 2.1495y - 0.45006y^2$
d_4	$-1.2970 - 0.13947y - 0.41197y^2 - 0.10641y^3$

Table 6: Parameters describing electron neutrino spectra for arbitrary proton energy.

Parameters	Formulae as functions of the proton kinetic energy ($y = \log_{10}(T_p)$) in TeV.
Non-diff., equation 6	
a_0	$0.0074087 + 2.9161(y+3.31) + 0.99061(y+3.31)^2 - 0.28694(y+3.31)^3 + 0.038799(y+3.31)^4$
a_1	$-3.2480 \cdot 10^{-5} + 7.1944 \cdot 10^{-5} \exp\left(-0.21814(y+3.4)\right) + 2.0467 \cdot 10^{-5}/(y+4.1640) + 5.6954 \cdot 10^{-6}y - 3.4105 \cdot 10^{-7}y^2$
a_2	$-230.50 + 58.802y - 9.9393y^2 + 1.2473y^3 - 0.26322y^4$
a_3	$0.45064 + 0.56930y + 0.012428y^2 - 0.0070889y^3$
a_4	$-0.011883 + 1.7992(y+3.32) + 3.5264(y+3.32)^2 - 1.7478(y+3.32)^3 + 0.32077(y+3.32)^4 - 0.017667(y+3.32)^5$
a_5	$-1.6238 \cdot 10^{-7} + 1.8116 \cdot 10^{-6} \exp\left(-0.30111(y+3.4)\right) + 9.6112 \cdot 10^{-5}/(y+4.8229)^2$
a_6	$-261.30 - 43.351 \log_{10}\left(0.35298(y+3.4)\right) + 70.925/(y-8.7147)^2$
a_7	$184.45 - 1473.6/(y+6.8788) - 4.0536y^2$
a_8	$-0.24019 + 0.38504y + 0.0096869y^2 - 0.0015046y^3$
$r(y)$	$0.329 \exp\left(-247((y+3.26)/(1+6.56(y+3.26)))^2\right) - 0.957y - 0.229y^2$ for $T_p \leq 7.81$ GeV
	1.0 for $T_p > 7.81$ GeV
Diffraction, equation 9	
b_0	$53.809 \tanh\left(-0.41421(y+2.2)\right) - 6.7538(y+0.76010)^2 + 0.0088080(y+8.5075)^4$
b_1	$-50.211 + 55.131 \exp\left(1.3651((y+1.8901)/(1.0+4.4440(y+1.8901)))^2\right)$
b_2	$-17.231 + 0.041100 \tanh\left(7.9638(y+1.9)\right) - 0.055449y + 2.5866 \cdot 10^{-4}(y+250.68)^2$
b_3	$12.335 - 12.893 \exp\left(-1.4412((y+1.8998)/(1.0+5.5969(y+1.8998)))^2\right)$
	Important: $b_0,\ldots,b_3 = 0$ for $T_p < 11.05$ GeV
b_4	$1.3558 + 0.46601(y+2.95) + 0.052978(y+2.2)^2 + 0.79575 \exp\left(-5.4007(y+2.2+4.6121(x+2.2)^2)^2\right)$
b_5	$1.8756 - 0.42169 \tanh\left(1.6100(y+1.9)\right) - 0.051026 * (y-3.9573)$
b_6	$1.5016 + 1.0118y - 0.072787y^2 - 0.0038858y^3 + 0.0093650y^4$
b_7	$4.9735 + 5.5674 \tanh\left(-0.36249(y+2.1)\right) - 0.20660 * (y-2.8604)$
$\Delta(1232)$, equation 12	
c_0	$2.8290 \exp\left(-71.339((y+3.1282)/(1.0+0.48420(y+3.1282)))^2\right) - 9.6339 - 15.733/y + 0.52413y^2$
c_1	$-24.571 - 15.831y - 2.1200y^2$
c_2	$-5.9593 - 6.4695 \tanh\left(4.7225(y+2.1)\right) + 0.50003y$
c_3	$0.26022 + 0.24545y$
c_4	$0.076498 + 0.061678y + 0.0040028y^2$
Res1600), equation 12	
d_0	$1.7951 \exp\left(-57.260((y+2.9509)/(1.0+1.4101(y+2.9509)))^2\right) - 0.58604 - 0.23868y$
d_1	$-2.6395 - 1.5105y + 0.22174y^2$
d_2	$-7.0512 - 7.1970 \tanh\left(31.074(y+2.1)\right) + 0.39007y$
d_3	$-1.4271 - 1.0399y - 0.24179y^2$
d_4	$0.74875 + 0.63616y + 0.17396y^2 + 0.017636y^3$

Table 7: Parameters describing electron anti-neutrino spectra for arbitrary proton energy.

Parameters	Formulae as functions of the proton kinetic energy ($y = \log_{10}(T_p)$) in TeV.
Non-diff., equation 6	
a_0	$0.0013113 + 0.36538(y + 3.31) + 1.5178(y + 3.31)^2 - 0.20668(y + 3.31)^3 + 0.024255(y + 3.31)^4$
a_1	$-4.7833 \cdot 10^{-6} + 4.5837 \cdot 10^{-5} \exp\left(-0.42980(y + 3.4)\right) + 6.1559 \cdot 10^{-6}/(y + 4.1731) + 1.1928 \cdot 10^{-6}y$
a_2	$-245.22 + 73.223y - 19.652y^2 + 0.083138y^3 + 0.71561y^4$
a_3	$0.45232 + 0.52934y + 0.010078y^2 - 0.0017092y^3$
a_4	$-0.0025734 + 0.38424(y + 3.32) + 1.5517(y + 3.32)^2 + 0.17336(y + 3.32)^3 - 0.17160(y + 3.32)^4 + 0.021059(y + 3.32)^5$
a_5	$4.7673 \cdot 10^{-5} + 5.4936 \cdot 10^{-5} \log\left(0.0067905(y + 4.3)\right) + 0.00020740/(y + 4.9772)$
a_6	$-270.30 - 114.47 \log_{10}\left(0.34352(y + 3.4)\right) + 80.085y - 7.9240y^2$
a_7	$3272.9 - 2.9161 \cdot 10^5/(y + 87.847) - 6.2330y^2$
a_8	$-0.17787 + 0.36771y - 0.025397y^2 + 0.0019238y^3 + 0.0032725y^4$
$r(y)$	$2.67 \exp\left(-45.7((y + 3.27)/(1 + 6.59(y + 3.27)))^2\right) - 0.301y - 0.208y^2$ for $T_p \leq 15.6$ GeV
	1.0 for $T_p > 15.6$ GeV
Diffraction, equation 9	
b_0	$41.307 \tanh\left(-0.37411(y + 2.2)\right) - 4.1223(y + 0.55505)^2 + 0.0042652(y + 9.2685)^4$
b_1	$-132.50 + 142.12 \exp\left(-8.0289((y + 1.9196)/(1.0 + 11.530(y + 1.9196)))^2\right)$
b_2	$-17.223 + 0.011285 \tanh\left(-69.746(y + 1.9)\right) - 0.048233y + 2.5881 \cdot 10^{-4}(y + 250.77)^2$
b_3	$8.1991 - 9.6437 \exp\left(-45.261((y + 1.9292)/(1.0 + 16.682(y + 1.9292)))^2\right)$
	Important: $b_0, \ldots, b_3 = 0$ for $T_p < 11.05$ GeV
b_4	$0.55919 + 0.36647(y + 2.95)^2 + 0.056194(y + 2.95)^4 + 0.49957 \exp\left(-5.5317(y + 2.2 + 0.43867(y + 2.2)^2)^2\right)$
b_5	$1.2544 - 0.52362 \tanh\left(2.7638(y + 1.9)\right) + 0.055837 * (y - 17.638)$
b_6	$1.4788 + 1.0278y - 0.092852y^2 - 0.0062734y^3 + 0.011920y^4$
b_7	$5.1651 + 5.7398 \tanh\left(-0.37356(y + 2.1)\right) - 0.22234 * (y - 2.7889)$
Res1600), equation 12	
d_0	$0.36459 \exp\left(-58.210((y + 2.9537)/(1.0 + 1.4320(y + 2.9537)))^2\right) - 0.11283 - 0.046244y$
d_1	$-9.5066 - 5.4655y - 0.31769y^2$
d_2	$-7.1831 - 7.1551 tanh(30.354(y + 2.1)) + 0.33757y$
d_3	$2.7938 + 1.6992y + 0.20161y$
d_4	$0.61878 + 0.62371y + 0.18913y^2 + 0.019118y^3$

Table 8: Parameters describing muon neutrino spectra for arbitrary proton energy.

Parameters	Formulae as functions of the proton kinetic energy ($y = \log_{10}(T_p)$) in TeV.
Non-diff., equation 6	
a_0	$-0.63611(y+3.3) + 9.9015(y+3.3)^2 - 4.5897(y+3.3)^3 + 0.91778(y+3.3)^4 - 0.060724(y+3.3)^4$
a_1	$6.8700 \cdot 10^{-6} - 2.8245 \cdot 10^{-6}y + 7.6032 \cdot 10^{-7}y^2 - 3.2953 \cdot 10^{-7}y^3 + 7.4292 \cdot 10^{-8}y^4$
a_2	$-240.46 + 58.405y - 9.8556y^2 + 3.1401y^3 - 0.88932y^4$
a_3	$0.49935 + 0.60919y + 0.0024963y^2 - 0.0099910y^3$
a_4	$2.5094(y+3.32) + 4.1350(y+3.32)^2 - 0.89534(y+3.32)^3 - 0.0027577(y+3.32)^4 + 0.014511(y+3.32)^5$
a_5	$8.2046 \cdot 10^{-7} + 1.4085 \cdot 10^{-6}\log_{10}(0.016793(y+4.3)) + 0.00013340/(y+4.7136)^2$
a_6	$-267.55 - 0.21018\log_{10}(0.35217(y+3.9)) + 69.586y - 9.9930y^2$
a_7	$2742.8 + 222.01\log_{10}(9.7401(y+3.9)) - 4772.5/(y+19.773) - 6.1001y^2$
a_8	$-0.11857 + 0.39072y - 0.037813y^2 + 0.0022265y^3 + 0.0046931y^4$
$r(y)$	$2.23\exp\left(-93.4((y+3.25)/(1+8.38(y+3.25)))^2\right) - 0.376y - 0.121y^2$ for $T_p \leq 15.6$ GeV
	1.0 for $T_p > 15.6$ GeV
Diffraction, equation 9	
b_0	$64.682\tanh(-0.34313(y+2.2)) - 5.5955(y+0.44754)^2 + 0.0050117(y+9.9165)^4$
b_1	$-7.6016 + 3.0427 \cdot 10^4\exp\left(-1.0134 \cdot 10^4((y+2.3066)/(1.0+41.612(y+2.3066)))^2\right)$
b_2	$-1.4978 - 0.58163\tanh(-0.36488(y+1.9)) + 0.031825(y+2.8097) + 0.022796(y-1.8861)^2$
b_3	$-0.0061483 - 65.799\exp\left(-4.8239((y+3.8835)/(1.0+0.53343(y+3.8835)))^2\right)$
	Important: $b_0, \ldots, b_3 = 0$ for $T_p < 11.05$ GeV
b_4	$2.8009 + 0.35341(y+2.95)^2 - 0.0039779(y+2.95)^4 + 1.3012\exp\left(-10.592(y+2.2-0.19149(y+2.2)^2)^2\right)$
b_5	$1.8016 - 0.69847\tanh(2.8627(y+1.9)) - 0.015722*(y-45.4)$
b_6	$1.4617 + 1.0167y - 0.078617y^2 - 0.0038336y^3 + 0.010141y^4$
b_7	$3.5599 + 4.0041\tanh(-0.41889(y+2.1)) - 0.18182*(y-2.4209)$
$\Delta(1232)$, equation 12	
c_0	$3.6052\exp\left(-60.914((y+3.1278)/(1.0-0.19497(y+3.1278)))^2\right) - 0.92514 + 2.1315/y + 0.23548y^2$
c_1	$95.310 + 70.497y + 13.636y^2$
c_2	$-6.2158 - 6.2939\tanh(21.592(y+2.1)) + 0.37440y$
c_3	$2.7485 + 1.1692y$
c_4	$-2.7568 - 1.8461y - 0.31376y^2$
Res1600), equation 12	
d_0	$2.5489\exp\left(-58.488((y+2.9509)/(1.0+1.3154(y+2.9509)))^2\right) - 0.83039 - 0.34412y$
d_1	$88.173 + 65.148y + 12.585y^2$
d_2	$-7.0962 - 7.1690\tanh(30.890(y+2.1)) + 0.38032y$
d_3	$-4.1440 - 3.2717y - 0.70537y^2$
d_4	$2.2624 + 1.1806y - 0.0043450y^2 - 0.043020y^3$

Table 9: Parameters describing muon anti-neutrino spectra for arbitrary proton energy.

Parameters	Formulae as functions of the proton kinetic energy ($y = \log_{10}(T_p)$) in TeV.
Non-diff., equation 6	
a_0	$-1.5243(y+3.3) + 10.107(y+3.3)^2 - 4.3126(y+3.3)^3 + 0.80081(y+3.3)^4 - 0.048724(y+3.3)^5$
a_1	$-2.6297 \cdot 10^{-5} + 9.3858 \cdot 10^{-5} \exp\left(-0.32384(y+3.4)\right) + 7.7821 \cdot 10^{-6}/(y+4.0560) + 7.6149 \cdot 10^{-6}y - 8.4091 \cdot 10^{-6}y^2$
a_2	$-223.62 + 59.374y - 5.7356y^2 + 1.9815y^3 - 1.0478y^4$
a_3	$0.50807 + 0.60221y + 0.0034120y^2 - 0.011139y^3$
a_4	$2.6483(y+3.32) + 4.4585(y+3.32)^2 - 1.2744(y+3.32)^3 - 0.11659(y+3.32)^4 + 0.0030477(y+3.32)^5$
a_5	$9.1101 \cdot 10^{-7} + 1.3880 \cdot 10^{-6} \log_{10}\left(0.016998(y+4.3)\right)1.2744 \cdot 10^{-4}/(y+4.7707)^2$
a_6	$-272.11 - 53.477 \log_{10}\left(0.35531(y+3.9)\right) + 56.041/(y-6.0876)^2$
a_7	$6431.8 + 893.92 \log_{10}\left(5.713 \cdot 10^{-9}(y+3.9)\right) + 2103.6/(y+5.6740) - 6.1125y^2$
a_8	$-0.11120 + 0.38144y - 0.040128y^2 + 0.0047484y^3 + 0.0054707y^4$
$r(y)$	$2.56 \exp\left(-107((y+3.25)/(1+8.34(y+3.25)))^2\right) - 0.385y - 0.125y^2$ for $T_p \leq 15.6$ GeV
	1.0 for $T_p > 15.6$ GeV
Diffraction, equation 9	
b_0	$70.430 \tanh\left(-0.35816(y+2.2)\right) - 6.6796(y+0.52273)^2 + 0.0065659(y+9.5266)^4$
b_1	$-8.1145 + 7686.0 \exp\left(4.4046 \cdot 10^4((y+2.2190)/(1.0+81.105(y+2.2190)))^2\right)$
b_2	$-1.3095 + 0.071270 \tanh\left(-0.0075463(y+1.9)\right) + 0.067759(y+5.3433) - 0.0044205(y-1.8683)^2$
b_3	$0.082149 - 2190.1 \exp\left(-533.75((y+2.8363)/(1.0+7.0976(y+2.8363)))^2\right)$
	Important: $b_0, \ldots, b_3 = 0$ for $T_p < 11.05$ GeV
b_4	$2.7540 + 0.33859(y+2.95)^2 - 0.0034274(y+2.95)^4 + 1.1679 \exp\left(-10.408(y+2.2-0.18922(y+2.2)^2)^2\right)$
b_5	$2.1817 - 0.59584 \tanh\left(2.7054(y+1.9)\right) - 0.010909*(y-14.9)$
b_6	$1.4591 + 1.0275y - 0.074949y^2 - 0.0060396y^3 + 0.0097568y^4$
b_7	$3.7609 + 4.2843 \tanh\left(-0.37148(y+2.1)\right) - 0.16479*(y-2.7653)$
$\Delta(1232)$, equation 12	
c_0	$2.8262 \exp\left(-62.894((y+3.1250)/(1.0-0.47567(y+3.1250)))^2\right) + 5.6845 + 13.409/y - 0.097296y^2$
c_1	$16.721 + 11.750y + 2.4637y^2$
c_2	$-6.0557 - 6.3378 \tanh(21.984(y+2.1)) + 0.43173y$
c_3	$0.37009 + 0.27706y$
c_4	$0.047507 + 0.061570y + 0.0070117y^2$
Res1600), equation 12	
d_0	$2.2400 \exp\left(-57.159((y+2.9492)/(1.0+1.2994(y+2.9492)))^2\right) - 0.66521 - 0.27554y$
d_1	$-7.0650 - 4.2773y - 0.17648y^2$
d_2	$-7.0410 - 7.1977 \tanh(31.095(y+2.1)) + 0.40238y$
d_3	$-1.2354 - 0.87581y - 0.20829^2$
d_4	$-0.11395 + 0.34418y + 0.27103y^2 + 0.050248y^3$